ADSORPTION OF COBALT, CHROMIUM, AND BARIUM ON RIPIDOLITE AND KAOLINITE AS EXAMINED BY X-RAY PHOTOELECTRON SPECTROSCOPY

by

Adrian Bruce Emerson

Thesis submitted to the Graduate Faculty of the
Virginia Polytechnic Institute and State University
in partial fulfillment of the requirements for the degree of

MASTER OF SCIENCE

in

Chemistry

APPROVED:

Dr. John G. Dillard, Chairman

Dr. James P. Wightman

Dr. Lucian W. Zelazny

Dec. 19, 1978

Blacksburg, Virginia

ACKNOWLEDGEMENTS

I would like to thank first of all, Dr. John G. Dillard, not only for his assistance in my research, but also for his encouragement and hospitality when I returned several times in order to complete my research. I also would like to thank the members of my committee; Dr. James P. Wightman and Dr. Lucian W. Zelazny for their aid in this investigation.

I want to take this opportunity to thank my wife, who not only assisted in my research, but whose love and understanding made a difficult job seem much less difficult. I would like to thank my parents, and , for their encouragement and understanding also.

The assistance of the Virginia Polytechnic Institute and State University Chemistry Department glass blowing shop (and) and the electronic shop (, and) was greatly appreciated. Finally I would like to thank Dr. James P. Wightman for his help with the BET surface area determinations and for his help with the adsorption experiments and the XPS measurements.

TABLE OF CONTENTS

Page

LIST OF TABLES

LIST OF FIGURES

1. INTRODUCTION

Each year, agriculture, industry, and every day activities account for the mobilization of 2.7×10^8 metric tons of solid material,[1] most of which enters into the ocean. Solid material is transported to the ocean by one of five means which are wind, glaciers, rivers, sewage and discharge from ships. The latter two are a direct result of human action and constitute about 10% of the solid material which reaches the ocean ecosystem. About $1\text{-}5 \times 10^8$ metric tons of solid material are transported to the oceans by the wind, while it is estimated that rivers transport approximately 140×10^8 metric tons of solid material.[1]

This suspended load is composed mostly of phyllosilicates various metal oxides and hydrous oxides. Kennedy[2] and Gibbs[3] report that greater than 95% of the clay mineral fraction is comprised of kaolinite, illite, montmorillonite and chlorite. These clay minerals adsorb trace metals which originate in ground water and runoff water.

Trace metals remain adsorbed onto the clay minerals until some change in the pH or ionic strength takes place. Kharka[4] et al. studied the adsorption of silver, selenium and cobalt on kaolinite, illite, chlorite, mica and metal hydrous oxides in distilled water. When placed in a sea water environment the clays desorbed as much as 70% of the adsorbed metal ion.

Riley and Chester[5] have pointed out the importance of understanding ion exchange processes on clay minerals. But knowledge of these exchange processes on clays is not complete.

The purpose of this study was to study the nature of the interaction of Co^{2+}, Cr^{3+}, and Ba^{2+} as a function of pH with the clay minerals ripidolite and kaolinite. X-ray photoelectron spectroscopy (XPS) was the experimental technique selected to examine this interaction.

The XPS technique is based on the general equation:

$$h\nu = E_b + E_k$$

where $h\nu$ is the energy of the incident x-ray radiation, E_k is the kinetic energy of the ejected electron, and E_b is the binding energy of the electron in the level from which it is ejected. XPS is capable of examining the extent that the positive or negative charge on a given atom changes by comparing the measured binding energy of a given element in several compounds with the known properties of the element in these compounds. Because the escape depth of the photoejected electrons is limited to the first 30Å of a sample surface, this technique has proven especially useful for surface analysis.

The adsorption of the cations was performed at constant pH so that the species in solution would be known. Then if changes in the species occurred, as the pH was

changed, XPS would be used to detect these changes on the surface of the adsorbent. This establishes a frame of reference for discussing why the binding energy differences occur.

Finally, the quantitative nature of XPS was compared with some atomic absorption data in order to demonstrate a correlation between them. The amount of cation removed from solution as determined by atomic absorption spectroscopy would be compared to a measure of the cation on the clay surface as determined from the cation/Si ratio. The cation/Si ratio was calculated from the XPS spectral data.

2. HISTORICAL

A. Definition and General Structure of Clays

The term clay is used to denote two basic meanings. On the one hand, it can denote any natural, earthy, fine grained material which develops plasticity when mixed with a limited amount of water.[6] Plasticity means that state when the moistened material can be deformed and the deformed shape retained when the pressure is removed. Some materials called clays which do not meet these specifications, such as flint clays, have no substantial plasticity when mixed with water.

The term clay has no generic significance. It is used for material that is the product of weathering, has been formed by hydrothermal action, or has been deposited as a sediment.[6]

Second, as a particle size term, the clay fraction can refer to the smallest size fraction of a soil or mineral analysis.[6] In geology, the $<4\mu$ particles are considered the clay fraction whereas those in soil science consider the $<2\mu$ particles to be the clay fraction. The $\leq 2\mu$ particle size fraction has gained wider acceptance as it has been found to be the best size split between clay minerals and other constituents.

This latter definition is also ambiguous because upon closer examination, a whole host of materials that are

unrelated structually exist in the so-called clay fraction. This leads to a consideration of a more fundamentally sound definition based on structure analysis.

The structures of clay minerals are diverse in nature and composition. However, an underlying groundwork is readily apparent when the structures are examined. The crystal structure reveals that two basic structural units make up almost all phyllosilicates. These structural units are tetrahedral sheets and octahedral sheets.

The tetrahedral sheets are composed primarily of silicon and oxygen (SiO_4) in tetrahedral coordination connected at three corners (Figure 1A) in the basal plane. The tetrahedra are arranged so that the apex of the tetrahedra all point into the silicate sheet (Figure 1B). This forms the silica tetrahedral sheet which looks like an open hexagonal network (Figure 1C). The O-O bond distance is ideally 2.55 Å; and the space available to an ion in the tetrahedral coordination site is about 0.55 Å.[6] The thickness of an undistorted tetrahedral unit is 4.65 Å in the clay mineral structure.[6]

The second structural unit consists of two planes of closely packed oxygens or hydroxyls in which primarily aluminum, magnesium or iron ions are in octahedral coordination (Figure 2). When aluminum is present, it is called the gibbsite sheet and only two thirds of the possible cation positions are filled to balance the charge. When magnesium is present, it is called a brucite sheet and all possible

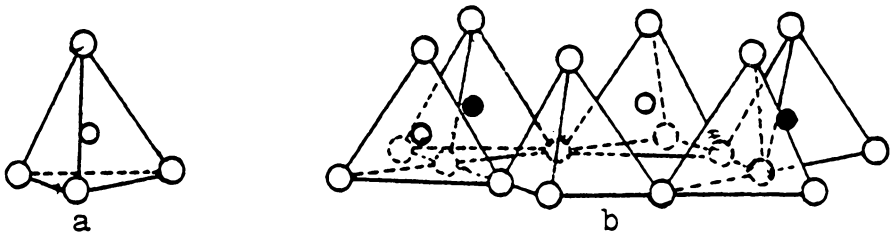

O and ○ = Oxygen ○ and ● = Silicon

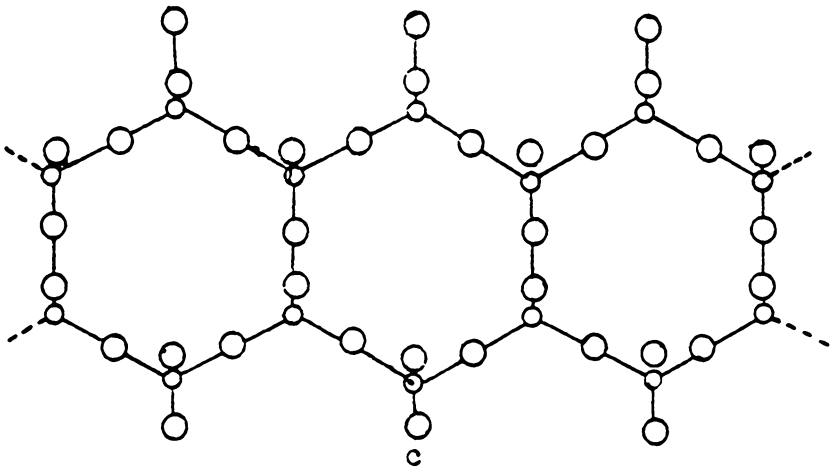

Figure 1. Typical clay tetrahedron, (a) typical tetrahedral clay sheet, (b) plane of silicon atoms from tetrahedral sheet forming a hexagonal network, (c)

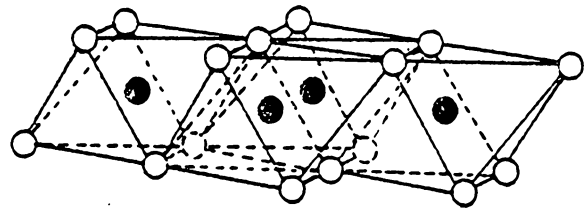

and ○ Hydroxyls ● Aluminum, Magnesium, etc.

Figure 2. Typical octahedral clay sheet

cation positions are filled.

The normal O-O bond distance is about 2.60 Å and the OH - to - OH bond distance is about 2.94 Å. The space available for octahedral coordination is about 0.61 Å and the theoretical thickness is 5.05 Å.[6]

The tetrahedral sheet projects into the octahedral sheet and coordinates with two-thirds of the appropriate anion. The major types of clays are based on the arrangement of the tetrahedral and the octahedral sheets. These types are 1:1 where a tetrahedral layer is projected into an octahedral layer, 2:1, where two tetrahedral layers are bound in such a manner that one is on either side of an octahedral layer, and a 2:1:1, where the central layer is the same as a 2:1 component with an additional octahedral sheet sandwiched in between each 2:1 layer in the inner layer position.

Additional subdivisions are based on:

1.) whether the octahedral layer has two cations per unit cell (dioctahedral) or three cations per unit cell (trioctahedral).
2.) the manner of stacking of the silica tetrahedral octahedral sheets (for example dickite and nacrite are both kaolin minerals with different stacking sequences).
3.) the amount and type of isomorphous substitution in the octahedral and tetrahedral layers.

B. Chemical Composition and Structure of Kaolinite

Kaolinite is a 1:1 type phyllosilicate and is a dioctahedral mineral having two aluminum cations in the octahedral layer. The chemical composition of an ideal kaolinite is

46.54% SiO_2, 39.5% Al_2O_3 and 13.9% H_2O. In nature, this exact composition is seldom found. Small amounts of impurities such as Fe_2O_3, TiO_2, MgO, CaO, K_2O, and Na_2O are present. Most samples also have either excess Al_2O_3 or SiO_2.[9]

Mineral impurities such as rutile, quartz, anatase, mica, feldspar, etc. are found with kaolinite in kaolins. Seldom is the analysis for these impurities sufficient to account for all of elemental impurities present.[7]

The structure of kaolinite was first proposed in general outlines by Pauling.[8] Later, Gruner[9] worked out the structure in some detail which was revised by Brindley and his colleagues.[10,11] More recent work by Newnham,[12] Brindley and Nakhira;[13] Bailey[14] and others has shown that the simple structure proposed in Figure 3 is modified by distortions in the lattice.

The general structure is composed of a single sheet of tetrahedral coordinated silica and a single sheet of octahedraly coordinated alumina combined so that the apex of the silica tetrahedra and alumina octahedra form a common plane. All the tips of the silica tetrahedra point in the same direction and coordinate with two thirds of the O or OH groups in the alumina octahedra. The aluminum atoms are considered to be placed so that adjacent aluminum atoms are separated by an O or OH group above and below, and making a hexagonal cation distribution in a single plane in the octahedral sheet. The remaining OH groups are placed so that each OH group is

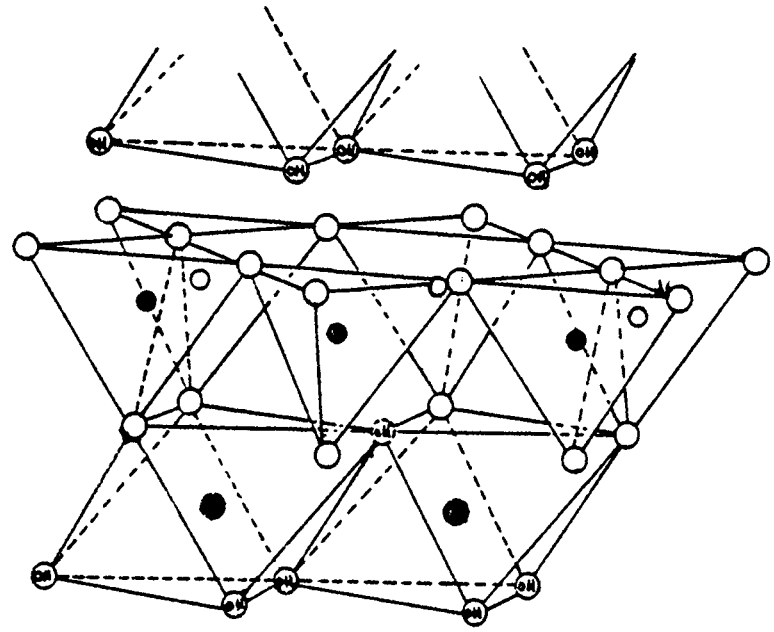

○ Oxygen

◉ Hydroxyls

● Aluminum

○ ● Silicon

Figure 3. Diagram of kaolinite structure

directly below the perforation of the hexagonal network of oxygens in the octahedral sheet.

The distortions are difficult to describe and will only be briefly treated here. The O groups common to the silica-alumina face are off center. The OH group is somewhat closer to the aluminum cations than shown. Also the OH bond is at an angle and not perpendicular to the silica-alumina interface plane. Further distortions in the octahedral sheet are caused by difficulties in fitting epitactually over the tetrahedral sheet. Kaolinite minerals are detected in x-ray diffraction studies by the common diagonistic peaks of 7.15 Å and 3.57 Å.[11]

C. Chemical Composition and Structure of Chlorite

Chlorite is a 2:1:1 type of phyllosilicates and can be either di, tri or tri, dioctahedral. The general structure is composed of alternate 2:1 like structure and a hydroxide structure. The layers are continuous in the a and b direction and stacked in the c direction. The general formula for the mica-like layer is $(OH)_4(Si.Al)_8(Mg.Fe)_6O_{20}$. The general composition of the hydroxide sheet is $(Mg.Al)_6.OH_{12}$.

An excess charge in the 2:1 layer is created by substitution of Al^{3+} for Si^{4+} in the tetrahedral sheet. The charge is balanced by an excess charge in the hydroxide sheet created by substitution of Al^{3+} for Mg^{2+}.

The structure of chlorite was first suggested by

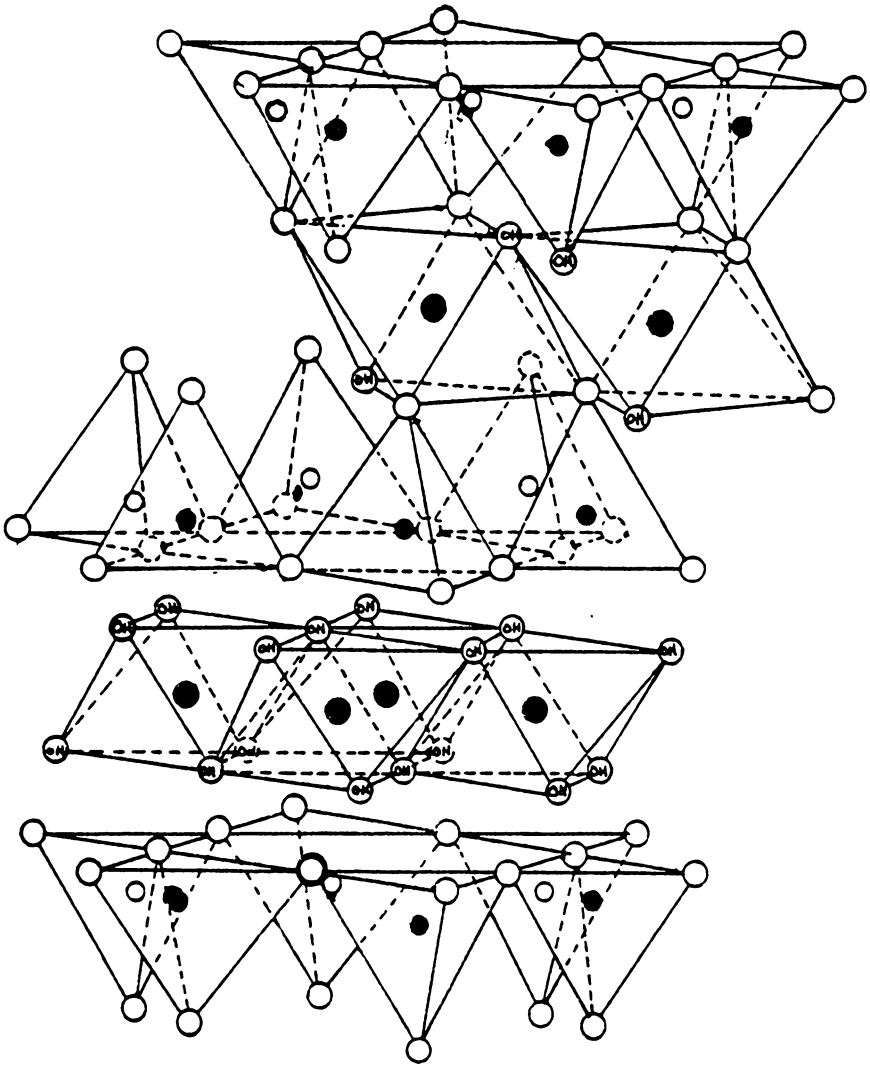

Figure 4. Diagram of chlorite structure

Pauling.[8] Later, Mauguin[15] and McMurchy[16] examined the mineral in greater detail, verified much of Paulings work, and provided much additional information on its symmetry and dimensions (Figure 4).

The bonding between layers is partly electrostatic in character as a consequence of substitutions within the lattice. A second important bonding mechanism arises from bonding between the hydroxide sheet and the tetrahedral sheet oxygens in the 2:1 layer. This bonding is similar to that in kaolinite.[6]

D. Adsorption and Ion Exchange Phenomena on Clay Minerals

The knowledge of ion exchange phenomena dates back many centuries. For example, peasants knew for centuries that liquid manures became decolorized and deodorized when passed through soils.[17] Serious study in the area of ion exchange did not begin until mid-19th century when Way and Thompson[18-20] began their studies of ion exchange. At that time, Thompson[18] studied fixation of ammonia on soils and Way[19,20] demonstrated that the active fraction in soils was composed of clay like materials. Since then, numerous studies of clays on nearly every aspect of ion exchange have been conducted.

Wilklander[21] defined cation exchange as a reversible process by which cations are exchanged between a solid substrate and its surrounding liquid phase. In this review, cation exchange and cation adsorption will be considered to have the same meaning.

Cation exchange is a result of a negative charge developed either on the faces or the edges of the clay particles. Grim[6] describes three ways charges develop:

1.) Broken bonds around the edges of the alumina-silicate units gives rise to unsatisfied charges on the surface edges. The broken bonds tend to be on noncleavage surfaces.
2.) Substitution within the lattice structure of cations of lower valence for those present, particularly Al^{3+} for Si^{4+} in the silica tetrahedra and low valence Fe^{2+} and Mg^{2+} for Al^{3+} in the octahedral layer.
3.) The hydrogens of exposed hydroxyls (which are an integral part of the structure rather than due to broken bonds) may be replaced by cations which might be exchangeable. This exchange might be important for kaolinite or hallosyte which have a basal plane of hydroxyls.

For kaolinite minerals, it is generally felt that broken bonds are the major cause of cation exchange capacity. However, Schofield and Somson[22] point out that only one silicon out of 400 need be replaced by Al^{3+}, to develop a cation exchange capacity (C.E.C.) of two milliequivalents per 100 gms of kaolinite.

There is enough excess aluminum present in most kaolinites for there to be 10 times this exchange capacity. Therefore substitution cannot be ruled out as the reason for cation exchange. Finally, the third possibility of basal hydroxyls interacting with cations at high pH cannot be ruled out as a reason for cation exchange either.

Although, all three reasons have some validity, most of the evidence supports broken bonds as the major source of exchange sites.[6]

For chlorite minerals, substitution in both the tetrahedral and octahedral layers accounts for most of the surface charge. Also, for chlorite and illite minerals of high crystallinity, broken bonds may contribute a major portion of the cation exchange capacity.[13]

Numerous studies of alkali and alkaline earth ion exchange on clays have been performed. These studies have been carried out in a variety of ways and with few exceptions, the order of exchange has been the same.

First, when considering negatively charged surfaces (clays for example) Swartzen-Allen and Matijevic[23] state three generalizations about ion exchange on these surfaces. The exchangeability increases (a.) with decreasing hydrated radius and increasing polarizability (b.) with increasing counterion charge and (c.) with decreasing ease of cation hydration. In cases of specific interactions with the surface, the above criteria do not apply.

Shainberg et. al.[24-26] reached this conclusion from conductance data on montmorillonite where they found that the relative strength of interaction was $Li^+ < Na^+ < K^+ < Rb^+ < Ca^{2+} < Cs^+$. For alkali ions the order of preference for ion exchange on montmorillonite,[27,28] vermiculite,[28] and kaolinite[29] was found to be $Li^+ < Na^+ < K^+ < Rb^+ < Cs^+$.

The order of exchange for alkali earth ions on clays has generally been found to be $Mg^{2+}<Ca^{2+}<Sr^{2+}<Ba^{2+}$.[30-32] The reverse order has been found for some vermiculites[33] and montmorillonites.[34] This anomalous behavior has been attributed to cation fixation, probably as a result of lattice collapse. The unit layers are held so tightly together that no interlayer exchange is possible.

Some cations because of specific interactions with the clay surface do not follow these orders. For example, cesium has shown anomalous behavior with respect to charge, sometimes being more strongly held than some divalent cations. Uskova and workers[35] found that for predominately H^+ saturated kaolinite, the exhibited preference was as expected but with predominately aluminum saturated kaolinite the order was reversed. Gal and Rich[36] also found that Cs^+ exchanged for Ca^{2+} to the near exclusion of Mg^{2+} in soil samples and some micas.

The same effect has been observed for competitive adsorption with potassium. The ease of removal of aluminum counterions from montmorillonites and kaolinite by various cations was found to be $Na^+<Ca^{2+}<K^+$.[37] It has been suggested that this effect is partly due to the size of the unhydrated potassium ion (1.33 Å), which permits it to take up a more favorable interlayer position.[38]

At high pH, the order of cation exchange capacity (CEC) magnitude is reversed for the alkaline earth

ions to $Ba^{2+}<Sr^{2+}<Ca^{2+}<Mg^{2+}$. This result has been explained by hydrolysis;[39] that is the more readily the ion is able to accept OH^- groups, the better it is adsorbed.

The adsorption of transition and heavy metal ions and complexes, is complicated by hydrolysis and hydroxylation effects which may occur in solution. Determination of the type of species, the type of bonding, and where bonding on the surface occurs has been investigated in a number of studies.

Numerous studies of Cu^{2+} adsorption have been performed on kaolinite, montmorillonite, and illite. In studies on kaolinite and illite, Farrah and Pickering[40-41] reached the following conclusions about Cu^{2+} adsorption. At pH>6 the clay suspension acts as a nucleation center for hydroxy bridged species. Second the major role of ligands is to mask the precipitation reactions and can be predicted from published data. Thirdly, the uncharged and negatively charged species are not adsorbed to any extent. Finally, the adsorptive capacity of the clay increases with increasing pH up to a limiting value of pH 7. For complex ions the CEC for singly and doubly charged species appears to be similar.

McBride[42] demonstrated through ESR studies that 30% of the adsorption sites on montmorillonite were relegated to divalent ions. These sites were postulated as resulting from disordered distribution of isomorphous substitution where two sites result from neighboring substitution.

A divalet cation would be bound more tightly in this type of site than two monovalent ions.

McBride[43] also studied Cu^{+} adsorption on kaolinite and concluded that edge sites were not responsible for cation exchange at least in the acidic range. It was reported that the cations were evenly distributed over the surface at an average of 11-12 Å. Other ESR studies[44] indicate that this effect might result from isomorphous substitution of Mg^{2+} for Al^{3+}. Numerous studies have also been performed with Co^{2+} on kaolinite, illite, montmorillonite, and on several oxides.

Murray[45] studied the adsorption of Co^{2+} on synthetic manganese dioxide, both as a function of pH and concentration of NaCl and sea water concentration of Mg^{2+}, Na^{+} and Ca^{2+}. Cobalt was chosen as the adsorbent because (1) it hydrolyzes to simple products ($Co(OH)^{+}$) (2) hydrolysis products are insignificant below pH 8 (3) it does not form polynuclear species and (4) it can be studied at low concentration using radioactive tracer techniques.

Murray[45] found that from pH 3 to pH 6, the Co^{2+} adsorption behaved as expected but from pH 6 to pH 8, the amount of Co^{2+} adsorbed was greater than hydrolysis products would predict. The sharp increase in adsorption was also coincident with a change of the surface charge from negative to positive as measured by electrophoretic mobility.

Healy et al.[46] investigated the adsorption of Co^{2+} at the silica/water interface as a function of pH and cobalt concentration. At a pH<6 and a concentration $<10^{-5}$M the adsorption was small. The cobalt ions were unhydrolyzed under these conditions. Between pH>6.5 but less than that necessary to precipitate $Co(OH)_2$ the data suggested some hydrolyzed species was adsorbed through an interaction of the form

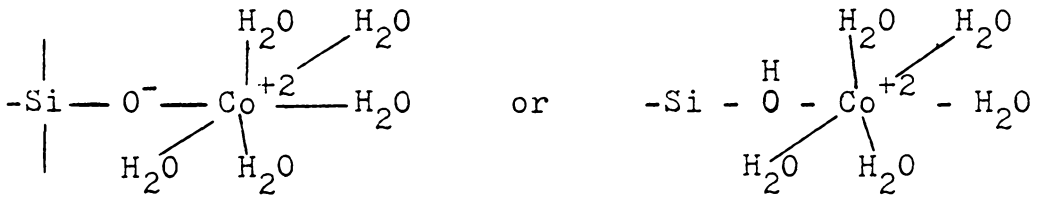

Tewari and Lee[47] studied the adsorption of cobalt (II) as a function of pH on TiO_2, ZrO_2, $NiFe_2O_4$ and Al_2O_3. They also found that cobalt adsorption increased abruptly between a pH of 6 and 8 and was probably due to hydrolysis of Co^{2+}.

Hildebrand and Blum[48] studied the uptake of lead on kaolinite, montmorillonite and illite. They found that in all cases the amount of lead adsorbed increased with increasing pH. Infrared studies of montmorillonite with lead adsorbed at pH 7 showed a reduction of a band at 2920 cm^{-1}. This band was attributed to the O-H stretch associated with the clay.

Forbes et al.[49] investigated the adsorption of the

complex ions $Co(NH_3)_6^{3+}$, $Co(NH_3)_5(H_2O)^{3+}$ and $Co(en)_2(H_2O)_2^{3+}$ on goethite. None of these complex ions adsorbed, not even when the latter two were hydrolyzed to hydroxo species. This lack of interaction was attributed to the strong stability of the Co(III)-OH bonds of the hydroxy ions which prevent formation of stable hydroxy-bridges between the oxide surface and the Co(III) species.

Swartzen-Allen and Matijevic[50] investigated the adsorption of $Co(dipy)^{3+}$, $Co(phen)_3^{3+}$ and Th^{4+} on Cs^+- and Na^+-montmorillonite by electrokinetic techniques. A charge reversal for the clay particles for all three ions occurs at about pH 3.5. Also Na-montmorillonite was a better adsorbent than Cs-montmorillonite. Further the uptake of the complexes exceeds the cation exchange capacity. Mechanisms in addition to simple ion exchange are responsible for adsorption of these complexes. This additional adsorption is due to chemisorption and causes the charge reversal on the clay particles.

Fordham[51] studied the adsorption of iron on kaolinite as a function of pH. The evidence indicated that from pH 2.2-2.7 the predominant species adsorbed was $Fe(OH)^{2+}$. In the pH region 2.7-3.6, the predominant species adsorbed was $Fe(OH)_2^+$. For pH values greater than 3.6 the adsorbed species was $Fe(OH)_3$. The factor deemed most important was that with the increase in pH, the actual form of the iron species was the controlling factor and not the change in

the surface of the kaolinite.

Dugger et al.[52] in a study of adsorption of cations on silica gel determined that the bond free energy of cations such as Ba^{2+}, Co^{2+}, and Cr^{3+} depends to a first approximation upon the charge density at the surface of the bare ion and not upon the electronegativity of the corresponding atom or the ability of the ion to form inner complexes. The free energy of the bond formed is proportional to log K for the association of the metal ion with one hydroxyl ion.

James and Healy[53] studied the adsorption of Cr^{3+}, Co^{2+}, Fe^{3+}, and Ca^{2+} on silica gel as a function of pH. Adsorption was found to show a steady trend with pH and concentration to saturation at the precipitation condition. The qualitative correlation between adsorption and hydrolysis was shown to break down when examined in detail. A complete description is shown to require many interactions for all hydrolysis products and the free ion.

In the review of studies of cation adsorption on minerals, many factors were found to affect that adsorption. To summarize, these factors were, the size and charge of the cation, pH of the solution, hydrolysis products, and the nature of the adsorbent surface.

E. X-ray Photoelectron Spectroscopy

The basic instrumentation of x-ray photoelectron spectroscopy is relatively simple. The spectrometer consists

of three parts; an x-ray source, a sample chamber, and an analyzer. The x-rays, which can be produced by several sources and are nearly monochromatic, bombard the sample causing photoejected electrons to leave the surface. These photoejected electrons pass into an analyzer which determines the energy of the electrons.

The kinetic energy of the photoelectrons expelled during this process is well defined. Any uncertainty or lack of definition of its energy is due to both the natural line width of the level from which the electron has been ejected and the inherent width of the incident radiation.[54]

XPS is a surface technique. Although the x-rays penetrate thru the bulk of the sample, the effective sampling depth is determined by the escape depth of the photoejected electrons. The escape depth varies from sample to sample and is dependent upon the energy of the incident radiation and the density of the sample to be studied. For most samples the escape depth is less than 50Å.[55-58]

The equation describing the photoejection process for solid samples is:

$$E_b = hv - E_k - \phi_{sp}$$

where E_b is the binding energy of the photoejected electron, hv is the energy of the x-ray photon, E_k is the kinetic energy of the ejected photoelectron and ϕ_{sp} is the function of the spectrometer. ϕ_{sp} is rarely determined as such,

but is treated empirically by calibration with a standard of known binding energy.

In the case of conducting solid samples, the determination of ϕ_{sp} is rather simple. In the case of nonconductors and semiconductors, a positive charge builds up on the sample surface as the photoejected electron leaves. In the case of semiconductors and insulators ϕ_{sp} includes not only the work function of the spectrometer, but may also include the extent of the charging on the surface.[54] Within the spectrometer, this surface charge is partially compensated by two mechanisms.[59] First photo conduction across the surface can occur with the spectrometer acting as a ground. Second, a return current to the sample is supplied by electrons formed from x-rays striking the interior of the spectrometer, most noticeably the window. However, some surface charge still exists on the surface.

A number of methods are used to correct for charging of the surface or Q_{ch}, but they all fall under two general categories; 1.) those which attempt to reduce Q_{ch} to a small value ($\leq$ .1ev) - for example, by using an extremely thin sample on conducting substrates or by flooding the sample environment with low energy electrons; 2.) those methods which use either internal or external methods to measure the magnitude of Q_{ch}. Each is described briefly below.

Ultrathin samples (one to several monolayers) are produced by a variety of methods and are studied on a

conducting support that is in electrical contact with the spectrometer. This method assumes that resistance to bulk electrical conduction will be sufficiently small to prevent charging. In all cases, the validity of the method must be checked using a flood gun, etc. to be sure that no small charging is occurring.[60]

In the flood gun[61] approach, the sample is bathed with low energy electrons which neutralize excess surface charge. The biggest disadvantage is that a negative charge can build up on the sample if the electron flux is too large or if the kinetic energy of the electrons is too great.

When considering internal or external standards, the general approach is to measure all spectra for each sample under a given set of instrumental parameters. For an external standard the apparent binding energy of a "standard" photoelectron level of some element not common to the sample is used for charge correction. However, for the external standard approach to be valid, the standard must be in electrical equilibrium with the sample. To determine if the external standard is in equilibrium with the sample a potential is applied to the sample and if the external standard photoelectron peak moves the same amount as the sample photopeak, they are in equilibrium.

The C 1s hydrocarbon peak at 285.0 eV, which is found nearly on all samples has been used most commonly in the past.[54] There is good evidence that the C 1s peak is in

electrical equilibrium with the sample since the C 1s photopeak moves the same amount as the sample photopeaks when a potential is applied. However, Lester and Dianis[62] feel that its use is not always valid, because the origin of the carbon is not always known. In new, "oil free" systems, the majority of the carbon originates from CO or CO_2.

An alternate approach has been the vapor deposition of a very thin gold film on the surface of the sample. The magnitude of Q_{ch} is determined by subtracting the apparent binding energy of the Au $4f_{7/2}$ peak from the true binding energy of the Au $4f_{7/2}$ peak. Except in the case of ultra clean surfaces, the vapor deposition proceeds by nucleation which forms islands of gold on the surface. However, it has been shown that these islands are usually in electrical equilibrium with the sample.[63]

Hercules, Betteridge and Carver[64] have shown that in some systems, the width and position of the gold peak changes with time of deposition, probe temperature, and sample. It was demonstrated that gold reacts with the surface of the sample.

More importantly, Riggs and Ginnard,[63] have shown that the amount of gold deposited is important. They found that as more gold is vapor deposited, the binding energy between the C 1s level and Au $4f_{7/2}$ level changes as much as 0.8 eV. In using gold deposition, care must be taken

to insure that a thin coverage is obtained and that approximately equal coverage of all samples is attained.

In the case of internal standards, an element present in the compounds to be studied is used as a reference. Because it is part of the lattice structure, it must be in electrical equilibrium with the sample. However, to be a valid reference, the reference element must not undergo a chemical shift from sample to sample. These conditions cannot be met often and greatly limit its applicability.

A good example of the use of internal standards is demonstrated by Olgivie and Wolberg[65] in their work on heterogeneous catalysts supported on alumina. They found that their precision was increased 3 to 10 times for copper, nickel and cobalt oxides when the Al_{2p} photoelectron line was used instead of the external C 1s photoelectron line.

Much of the early interest in XPS came about from the recognition that the exact binding energy of a photoelectron of a given atom was related to the amount of charge on it. Siegbahn[54] called this relationship the chemical shift which he defined as the difference in binding energy of a given core electron in an atom for two different compounds. It was demonstrated that the chemical shift of a particular element could be related to its oxidation state and its geometric environment.[54]

From purely electrostatic arguments, the greater

the amount of positive charge on an atom, the higher the binding energy of its photoelectrons.[54] However, when considering solid samples, the effect of the crystal potential must also be considered. For comparison of binding energies and correlating them to changes of the atomic charge, the crystal site potential must be essentially equivalent for samples being compared.

Also of interest when considering 1st row transition metals is satellites. These satellites can be attributed to three processes.[66]

1.) Auger electron excitations.
2.) Multiplet splitting, where the core hole state couples with an unpaired valence electron.
3.) "Shake-up" or "Shake-off" processes where the photoionization process simutaneously causes ionization or excitation of the valence electrons

These satellites have been observed in all of the paramagnetic complexes in the first row. The satellites can also be used to aid in determining what oxidation state the element in question is, and what type of bonding is occurring.[67]

In an XPS investigation of minerals Yin et. al.,[68] found that only one type of oxygen existed in olivine, whereas, pyroxenes contained two oxygens. The intensity ratio of the two oxygens in the pyroxenes was 2:1 with a binding energy difference of 1 eV. It was postulated that these two oxygen types were the result of a binding energy

difference between non-bridging and bridging oxygens within a silicate mineral.

Adams et al.[69] determined the binding energies of Fe, Mg, Al, Si, and O for a number of well characterized silicate minerals. No significant binding energy shift between Fe^{2+} and Fe^{3+} was found. Also the O 1s line widths were found to be narrower for minerals with one type of oxygen than for ones with two or more types.

Also, an XPS study[70] of minerals with magnesium in 2, 4, and 6 coordination showed strong shifts in the binding energy. A nearly linear correlation was found between the binding energies and the average magnesium-to-oxygen distance.

A number of investigations of lunar materials have also been carried out using XPS. Huntress and Wilson[71] obtained rapid, nondestructive, elemental (qualitative) analysis of lunar samples. The iron in the lunar samples was found to have a chemical shift similar to iron in the Fe^{2+} state.

Schultz et al.[72] demonstrated that XPS could be used to differentiate between silicate minerals on the basis of the chemical shift in the Si 2_p level. Five different silicon environments in coal and three silicon environments in respirable coal dust were reported. Also it was possible to differentiate between the more hazardous silicates and those that were virtually harmless.

Counts et al.[73] used XPS techniques to perform the first studies of adsorbed metals on minerals. Adsorption from aqueous solution of lead onto montmorillonite was studied. A comparison of the adsorbed lead with lead dioxide, lead oxide and elemental lead was made. It was concluded that the adsorbed lead was similar to lead oxide.

Koppelman and Dillard[74] studied the adsorption of Fe(III) and Cr(III) from aqueous solution onto clay minerals. The binding energies of the lattice elements of illite, kaolinite and chlorite were reported. The deconvolution of the iron photopeak of illite into Fe^{2+} and Fe^{3+} demonstrated the applicability of XPS to determine Fe^{2+}/Fe^{3+} ratios. A later study[75] of the adsorption of Cu(II) and Ni(II) was performed on kaolinite, illite and chlorite. Examination of the mode of bonding of the metal ions to the clay with XPS showed that Ni(II) was adsorbed as the aquo ion while Cu(II) was adsorbed as the $Cu(OH)^{+}$ species. Binding energies of Cu and Ni minerals were reported.

Stucki[76] et al. analyzed nontronite and biotite by XPS. Both minerals yielded good XPS spectra with well defined peaks. The elements identified from the XPS spectra were in good agreement with molecular formulas. From high resolution scans, the binding energies for Fe^{3+} were determined at 711.8 eV in dithionite reduced nontronite and in oxidized biotite. Peaks for Fe^{2+} occurred at 710.0 eV for unaltered biotite; at 709.0 eV for oxidized biotite, and

at 708.6 eV for hydrazine-reduced and dithionite-reduced nontronite. The O 1s peak for unaltered nontronite was skewed to the high energy side of the 530.6 eV maximum, but became more symetrical as the Fe^{2+} content increased.

In a later study, Stucki, Roth, and Baitinger[77] studied the oxidation-reduction mechanism for structural iron in nontronite. A two step mechanism was proposed from XPS, Mossbauer and CEC data. First, an initial reduction of Fe^{3+} to a Fe^{2+} content of 53 mmoles/100 gms. with an accompanying increase in layer charge and no structural change was suggested. Next, there is a further reduction to a Fe^{2+} content of 139 mmoles/100 gms. during which a constant layer charge is maintained by the elimination of structural OH and the coordination number of Fe in nontronite is decreased. The Fe^{3+} binding energy for oxidized nontronite and hydrazine reduced nontronite was 711.8 eV. The Fe^{3+} binding energy for dithionite reduced nontronite was 711.0 eV. The Fe^{2+} binding energy for both dithionite and hydrazine reduced nontronite was 708.6 eV.

Tewari and Lee[47] reported on the binding energy of Co^{2+} adsorbed on various oxides. The XPS spectrum of cobalt adsorbed on ZrO_2 or Al_2O_3 corresponds closely to that for $Co(OH)_2$. They related the increased adsorption of Co^{2+} to the precipitation of $Co(OH)_2$ as shown by the XPS spectra.

Briggs and Bosworth[78] challenged the interpertation of the cobalt spectra of Tewari and Lee[47] for two reasons.

First, it was not enough to compare the binding energies of Co $2p_{3/2}$ to determine the chemical oxidation state. Instead one should examine the distance between the Co $2p_{1/2}$-Co $2p_{3/2}$ peaks. For high spin Co^{2+} and low spin Co^{3+} compounds there is a $2p_{1/2}$-$2p_{3/2}$ separation of 16.0 and 15.0 eV, respectively.

Second, the importance of considering the surface contamination of the metal oxide standards is discussed, specifically that CoO has some Co_3O_4 on it. The contamination was deduced from low satellite intensity of the 2p peaks. After argon induced reduction of the "as received" CoO, the Co 2p two spectra had the expected high satellite intensity.

In reply, Tewari and McIntyre[79], stated that their procedure had been to identify the chemical state of Co by the presence of major shake-up satellite for Co^{2+} compounds whereas they are weak for Co^{3+} compounds. Once the chemical state was identified, the use of binding energies was considered acceptable in determining whether the Co^{2+} compound was CoO or $Co(OH)_2$. The Co $2p_{1/2}$-Co $2p_{3/2}$ spacing was checked and the results did not change their interpretation published earlier.

Lunsford[80] et al. studied cobalt nitrosyl complexes on zeolites A, X, and Y. Infrared and XPS data suggested that no appreciable electron transfer between the metal ion and the ligand occurred, whether the complex was mono or dinitrosyl.

Sommer[81] studied the C 1s and O 1s levels of various carbonate minerals. It was demonstrated that as covalency increases, the O 1s binding energy increases in calcite, magnesite, and otavite. However, the O 1s binding energy decreases in aragonite, strontionite and witherite. No increase in the line width was detected for O or C from the two sites in dolomite.

McIntyre and Cook[82] studied the XPS spectra of simple and mixed oxides and hydroxides of copper, cobalt, and nickel. The divalent oxides of these metals can be distinguished from the analogous hydroxides. The materials are distinguished by 1.) the distinctively larger chemical shift of the metal core peaks for the latter, 2.) by the energies of the satellite peaks and 3.) by the differences in binding energies of the O 1s level. Mixed oxides are sometimes identifiable on the basis of the satellite structure as well as the O 1s binding energy.

Oku and Hirokawa[83] examined x-ray photoelectron spectra of Co, Ni, and Cu 2p levels for samples of $M_xM_{1-x}O$ (M = Co, Ni, Cu), and CoO, CuO, and NiO. The binding energies of the metal $2p_{3/2}$ levels did not change with their concentration. The shake-up satellites/main peak intensity ratios and FWHM of the metal $2p_{3/2}$ levels of Co^{2+} and Cu^{2+} in MgO were smaller than those of CoO and CuO. The Ni $2p_{3/2}$ spectrum for Ni^{2+} in MgO had no shoulder, unlike NiO. These results indicated that the next nearest

neighbor ions (metal ions) may influence the final states after photoelectron ejection.

Nordberg[84] et. al. reported the binding energy of "2p" electrons of silicon in 16 compounds. The binding energies were discussed in view of the elements surrounding the silicon atom. It was found that the binding energies ranged from 107.4 eV for Na_2SiF_6, in which the silicon atom is surrounded by strongly electron-withdrawing atoms, to approximately 99 eV for the element.

Allen et al.[85] used XPS to study chromium oxygen systems. It was shown that the ionization energy of the chromium 2p electrons is dependent primarily on the oxidation of the chromium metal ion, but small perturbations in the binding energy within the same oxidation state may be attributed to change in the crystal structure.

XPS is also capable of producing semiquantitative information about the elements on the sample surface. This is normally accomplished by comparing the relative intensities of the elements of interest. Many papers on this subject have been published but only a few of special interest will be reviewed.

Wagner[86] investigated several of the factors which affect XPS measurements. It was determined that elements other than transition metals can be determined with a standard deviation of 10% if photoelectrons of similar energy are used. Larger errors result from using lines of widely

different energies because of variations in mean-free path ratios among materials; and more importantly surface contamination. Transition metals pose special problems because of the prevalence of multi electron processes.

Petrovic[87] et al. studied the dissolution of feldspar grains by XPS. Sanidine grains were subjected to dissolution in aqueous solutions of pH ranging from 4 to 8. Dissolution equivalent to the removal of the first 300 to 900 Å was accomplished. The surface of the reacted feldspar was found to be the same elemental composition as that of the reacted feldspar. It was concluded that the dissolution was not controlled by diffusion through a tightly adhering protective layer of hydrous aluminum oxide, kaolinite, or decationated feldspar, as was suggested by previous studies. Instead the kinetics is controlled by processes occurring at the fresh feldspar/solution interface.

Adams[88] et al. studied several alumino silicates and other solids by XPS. It was shown that XPS is capable of providing bulk quantitative analyses of air stable homogeneous solids. Accuracies of up to 5% on the average, were obtained for main group elements, provided that the use of low kinetic energy photoelectrons (<800 eV) is avoided and care is taken to avoid contamination of the surface.

Bancroft et al.[89] did a calibration study for quantitative XPS of Ba^{2+} and Pb^{2+} on calcite crystals. Linear reproducible calibration plots of monolayer and

submonolayer amounts of Ba^{2+} and Pb^{2+} on cleaved calcite surfaces were made. It was possible to detect a small fraction of the monolayer (10^{-9} gm/cm^2) of Ba^{2+} or Pb^{2+} on the calcite surface. Although there was a carbon film contaminating the surface of the calcite crystals, the slope of both the Pb^{2+} and Ba^{2+} plots were in semiquantitative agreement with theoretical estimates.

Further information about the basic principles and applications of XPS can be obtained from several review articles.[90-92]

The purpose of this research was to investigate the adsorption of metal ions on clay minerals using XPS. As has been suggested previously, a great amount of information exists regarding the amount of metal ions a clay may adsorb. However, little information exists regarding the metal ion to clay bond or the chemical nature of the adsorbed species.

XPS is especially appropriate for this type of investigation since it is sensitive to the electronic environment of an atom. Also because adsorption is a surface phenomena, the sampling depth of XPS is very appropriate, generally being less than 50Å.[55-58]

The metal ions Co^{2+}, Cr^{3+}, and Ba^{2+} were chosen for the adsorption study. Adsorption was studied as a function of pH. Co^{2+} and Cr^{3+} were chosen because the species in solution for these two cations are well characterized as a function of pH. Also if changes in binding energy did occur

it was hoped that it could be determined whether these changes were a result of change from physical adsorption of the cation on the clay surface to chemical adsorption as has been proposed by some,[48] or whether a change in the cation species adsorbed[47] would account for a binding energy change.

The study of Ba^{2+} adsorption was also undertaken to help determine which of these two mechanisms would be more probable. Finally, a comparison of the quantitative nature of XPS was made with atomic absorption data where possible in order to see if any correlation between the results could be made.

3. EXPERIMENTAL METHODS

A. Mineral Characteristics

1.) Kaolinite

The kaolinite used in the adsorption and XPS studies was a Georgia kaolinite received from Georgia Kaolin Corporation and designated Hydrite-R. The chemical composition is summarized in Table I and was determined by Georgia Kaolin. The mean particle size is 0.77μ and greater than 90% of the kaolinite is less than 3μ. The kaolinite was used as received in all of the experiments. X-ray diffraction data (Table II) confirmed that the sample was kaolinite. Cation exchange capacity and BET surface areas are presented in Table III.

2.) Ripidolite

Ripidolite, the chlorite mineral chosen for both the adsorption and XPS studies came from Flagstaff Hill, El Dorado County, California. It was purchased from the Source Clay Minerals Repository, Department of Geology, University of Missouri, Columbia, Missouri. Ripidolite was received in chunks several inches long and about an inch in thickness and in width. Visible iron oxides were removed by scraping. The chunks were broken into smaller pieces so that the pieces would fit into a Wig-L-Bug capsule. The ripidolite was ground up in the Wig-L-Bug for 30 seconds. Chemical composition data is

Table I

Clay Chemical Compositional Analysis

	Kaolinite	Ripidolite
SiO_2	45.30 %	25.8 %
Al_2O_3	38.38	18.3
Fe_2O_3	0.30	4.1
FeO	*	21.3
TiO_2	1.44	*
CaO	0.05	-
K_2O	0.04	-
Na_2O	0.27	-
MgO	0.27	20.3
H_2O	13.97	8.7
	98.02	98.5

* - not analyzed

Table II

X-ray Diffraction Peaks for the Clay Minerals

2θ values

Kaolinite		Ripidolite	
Experimental Values	Lit. Values*	Experimental Values	Lit. Values*
12.03	12.34	6.05	6.27
24.45	24.88	12.30	12.52
37.45	37.71	18.65	18.78
50.80	51.02	25.00	25.18
62.18	62.75	31.50	31.65

* Selected Powder Diffraction Data for Minerals[95]

Table III

Clay Adsorbent Characteristics

Clay	BET Surf. Area m^2/gm	CEC. meq/100gm
Kaolinite	12	7
Ripidolite	1	2

given in Table I. X-ray diffraction data (Table II) confirmed that this was a relatively pure chlorite. B.E.T. surface area and cation exchange capacity data are summarized in Table III.

3.) Volkanskoite

Volkanskoite, a chromium containing clay mineral was provided by Dr. Mitchell Koppelman of Georgia Kaolin. This mineral was used in XPS studies only to determine the binding energy of chromium. The chromium photoelectron peak was referenced to the C 1s photoelectron peak. The samples were ground in a Wig-L-Bug.

B. Test Solution Preparation

All metal ion solutions used in the adsorption experiments were 100 ppm and were made from the following salts: $Co(NO_3)_2 \cdot 6H_2O$ (Baker Analyzed) and $Cr(NO_3)_3 \cdot 9H_2O$ (Fisher Certified). A measured volume of double distilled, deionized water was heated to 65°C in a Pyrex flask. While cooling, argon was bubbled through a glass tube with a fritted end to saturate the water with argon. When cooled, the nitrate salt was added and the pH adjusted. pH was measured with a Model # 4094 L-25 Fisher combination electrode in conjunction with a Corning Model 703 pH meter. The electrode was standardized with pH 4 and pH 7 buffer solutions saturated with nitrogen. The pH was considered constant when the pH did not change by more than 0.05 pH

units after 10 to 15 minutes. The pH was adjusted using dilute solutions of either HNO_3 (0.1N) or NaOH (0.1N).

C. Preparation of the Reaction Mixture

Approximately 2.500 grams of clay was weighed out on a centigram balance (±5mg) and placed in the reaction vessel. The reaction vessel was the same as used in a previous study[93] with one modification. An extra septum inlet was placed opposite to the one already present so that a combination pH electrode could be introduced (Figure V). A Teflon stirring bar was added and both inlets sealed with rubber septa. The vessel was evacuated to 10^{-4} torr and then pressurized to approximately 850 torr with argon. A 500 ml. aliquot of the appropriate metal ion solution was added to the vessel and argon bubbled in the solution for approximately one minute to remove any trapped air in the vessel. The vessel was then repressurized to 850 torr with argon. The reaction vessel was attached via a ball and socket joint to a vacuum manifold located over a constant temperature bath (25.0 ±0.1°C) and submerged below its solution level. The pH was checked immediately before insertion into the tank since there was almost always a fast initial change, especially for kaolinite. Those systems which did not exhibit a fast initial change were those clay samples that were started at pH 2 or pH 4. The pH was checked again 3-5 hours later and subsequently every 12 to 24 hours.

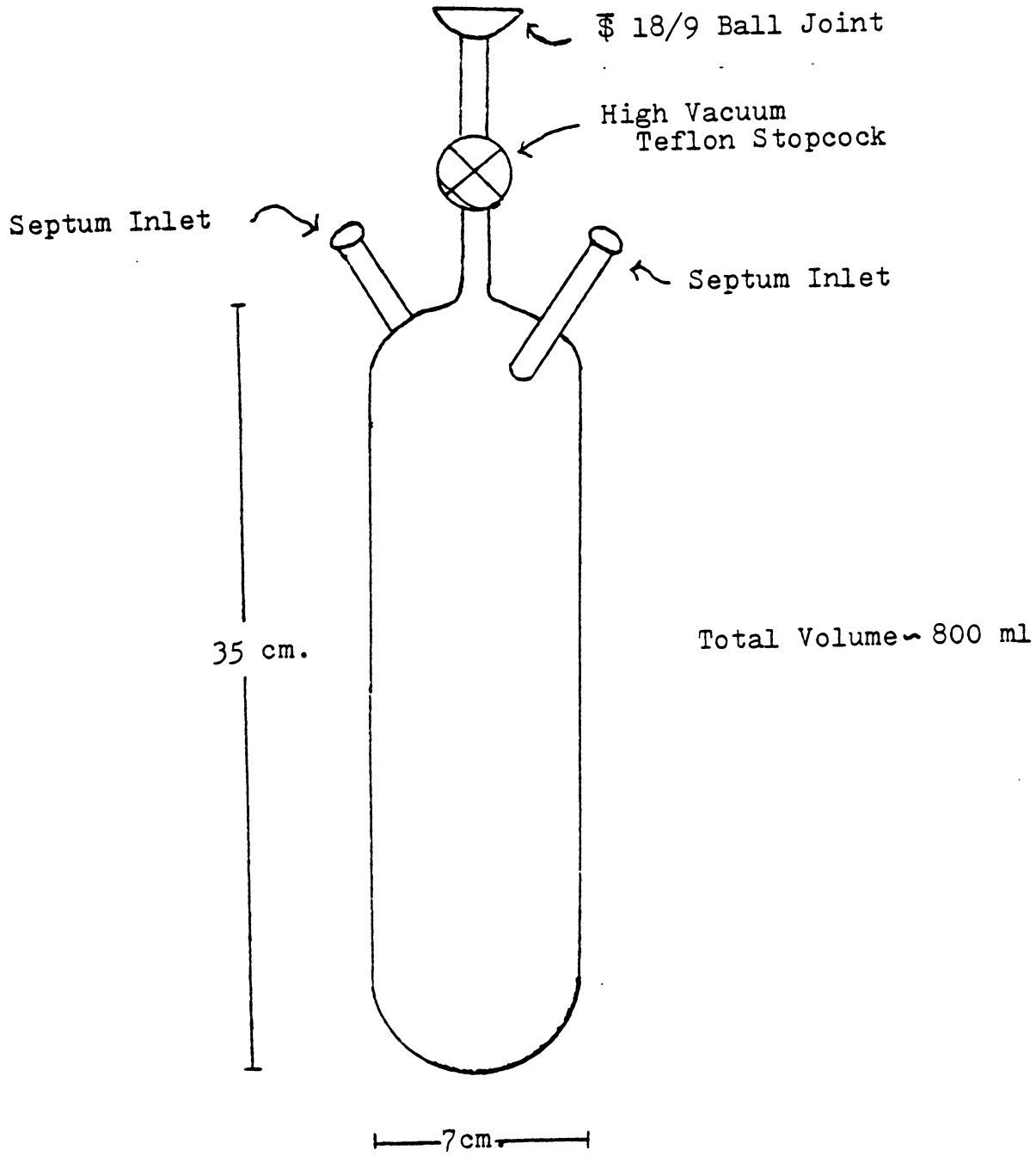

Figure 5. Sample vessel

At each measurement, the pH was adjusted when it varied more than ±.15 pH units from the desired pH value by adding HNO_3 (0.01 N) or NaOH (0.01 N) to the vessel. These solutions were prepared from degassed water to insure removal of carbonates and oxygen and were stored in polyethylene bottles.

The pH was checked after all suspended matter had settled (except in the first measurement) by inserting the pH electrode through the septum inlet. Positive pressure was maintained in the reaction vessel to exclude air.

The total contact time was 7 days (168-175 hours) and upon completion, an aliquot for analysis was taken. The solutions were separated from the adsorbent by centrifuging the suspension in an International Clinical centrifuge at approximately 1000 rpm at ambient temperature until the solution was visibly clear. The clear solution was decanted from the adsorbent, and the adsorbent placed in a vacuum dessicator to remove water.

D. Analytical Determinations

Dissolved silica was determined spectrophotometrically using the silicon-molybdate method.[93] For dissolved silica concentrations less than 10 ppm, the silicon molybdate complex was reduced using p-methyl amino phenyl sulfate as the reducing agent. The blue reduced complex was analyzed on a Beckman DU spectrophotometer at

a wavelength of 810 nm.

For dissolved silica concentrations between 10 and 50 ppm, the yellow complex was left unreduced and analyzed at a wavelength of 404 nm. The calibration plot was linear in the indicated concentration range.

The concentrations of the elements Al, Mg, Fe, K, Co, and Cr were determined by atomic absorption spectrophotometry. A Perkin-Elmer Model 503 atomic absorption unit was used through courtesy of the Soils Testing Lab, Agronomy Department, Virginia Polytechnic Institute and State University, Blacksburg, Virginia.

Single element hollow cathode lamps were used to determine Al (Perkin Elmer), and Mg (P.E.). Multielement lamps were used to determine the remaining elements: Na-K (P.E.) and Cr-Cu-Co-Mn-Fe-Ni (Fisher Scientific).

Standards prepared from stock 1000 ppm solutions were used to calibrate the atomic absorption spectrophotometer. By using less sensitive wavelengths and adjusting the angle of the burner head, the linear concentration range could be extended. Working linear ranges used were similar to those employed by Koppelman.[93] Experimental parameters used for atomic absorption(AA) analysis are presented in Table IV.

Concentrations for elements determined by AA are given in the tables in the results and discussion section. The precision of the atomic absorption measurements was $\pm$ 1 ppm.

Table IV

Atomic Absorption Spectrophotometer Settings
for Sample Solution Concentration Determinations

Element	Flow Type		Slit	Range	Conc.	Burner Head (relative to light beam)
Al	N_2O-C_2H_2	309.6	4	UV	0-100	parallel
Si	N_2O-C_2H_2	251.8	3	UV	0-1000	parallel
Fe	air-C_2H_2	248.0	3	UV	0-5	parallel
		374.0	3	UV	5-100	parallel
Mg	air-C_2H_2	285.5	4	UV	0-50	70°
K	air-C_2H_2	382.8	4	VIS	0-200	parallel
Co	air-C_2H_2	241.1	4	UV	5-100	70°
Cr	air-C_2H_2	213.4	4	VIS	5-100	parallel

The amount of Co^{2+} or Cr^{3+} removed from solution was calculated from the equation:

$$M^{x+}\text{adsorbed} = M^{x+}\text{intial} - M^{x+}\text{final}$$

where M^{x+}adsorbed represents the amount of Co^{2+} or Cr^{3+} removed from solution in ppm (mg/liter), M^{x+}intial represents the measured concentration of Co^{2+} or Cr^{3+} in ppm (mg/liter) at the beginning of the experiment, and M^{x+}final represents the final measured concentration of the solution in ppm (mg/liter) at the end of the adsorption experiment. This final concentration of Co^{2+} or Cr^{3+} was converted to the more commonly used CEC term of meq per 100 grams by the equation:

$$\frac{(M^{x+}\text{ adsorbed})\ (V)\ (40)X}{\text{Atomic wt. } M^{x+}} = M^{x+}\text{ adsorbed in meq./}_{100}\text{ gms}$$

where M^{x+}adsorbed represents the amount of Co^{2+} or Cr^{3+} adsorbed in mg/liter, V represents the volume of the solution used in the experiment in liters, X represents the charge on the cation, and Atomic wt. M^{x+} represents the atomic wt. of Co^{2+} or Cr^{3+}.

E. Barium Adsorption Experiment

A 100 ppm $Ba(NO_3)_2$(Fisher Certified) was prepared in doubled distilled deionized water. 500 ml. of this solution was added to 2.500 gms of kaolinite and ripidolite in an Erlenmeyer flask and the solutions kept at ambient temperature.

The pH was adjusted as described previously. The total contact time was five days. The solutions were separated from the adsorbent by centrifugation and then the adsorbent was placed in a vacuum dessicator to remove water. Because the original intention of the experiment was that of checking binding energy differences only, no attempt was made to determine the amount of Ba^{2+} adsorbed from solution.

F. Physical Instrumentation and Measurements

X-ray diffraction patterns were obtained from oriented samples on ceramic tiles. The samples were placed on the tile by vacuum suction by a method developed by Rich.[94] A Diano 8000 XRD x-ray diffractometer emitting Cu K_α radiation employing a graphite monochromator was used with a scanning speed of 2°/min. X-ray patterns were compared with those tabulated in the Selected Powder Diffraction Data for Minerals.[95]

XPS measurements were made using an AEI Model ES100 and a Dupont Model 650 photoelectron spectrometers. The AEI-ES 100 spectrometer consists of 3 basic units, a spectrometer unit, an electronic controls unit and an x-ray generator. The spectrometer unit has a multiaccess sample chamber with a port for introduction of solid samples. Also it contained the x-ray filament and target (Al).

The photoejected electrons pass through a lens system into a hemispherically shaped electrostatic

analyzer and are detected using a Spiraltron electron multiplier. The pulse from the multiplier is amplified, sent to the electronic controls unit and stored in a computer.

The data was collected by a Digital Equipment Corporation PDP 8/e computer in conjunction with the AEI-DS 100 software and hardware system. This data system was equipped with both wide (>400 channels) and narrow (<400 channels) scanning capabilities. A variable binding energy step is available in the scanning program. A scan of 150 channels with a -0.1eV binding energy step, the scan would be for 15 eV from higher to lower binding energies. Counting times were typically 3-4 seconds per channel for adsorbed elements and 1-1/2 seconds per channel for the internal reference (silicon) standard.

Samples with adsorbed cobalt were scanned for 12-36 hours and chromium samples were scanned for 6-12 hours. The data was punched out on a paper tape and pertinent data statistics for the scan were printed out on a teletype. The paper tape was used to plot the data on a Hewlett-Packard Model 2D-2AM X-Y recorder in conjunction with a DS-32 and/or a floppy disc unit. The MADCAP IV* program was used to smooth and plot the data. An 11 point smoothing

*MADCAP - A Multiplexed ADC and Analog Plotter Program. Written by G.W. Dulaney, presently at Digital Equipment Corp., Maynard, Mass.

routine was used to smooth the data points. A line plot was then drawn through the smoothed data points.

Samples were introduced on a copper probe which had 4 rectangular sides, one of which was gold plated. Each side was 7 mm by 30 mm. All samples were put on the side which was gold plated. The probe was introduced into the chamber by mounting it on a cylindrical steel shaft which was then inserted through o-rings and a Goddard valve.

The vacuum, which was generally $<10^{-6}$ Torr was obtained using two mechanical pumps and two oil (polyphenyl ether) diffusion pumps. Back streaming of the oil into the sample chamber and analyzer is minimized by water cooled baffles and by cyrogenic (liquid nitrogen) traps mounted over the oil diffusion pumps.

The Dupont 650 spectrometer consists of a spectrometer, electronic controls unit and a plotter. The spectrometer was made up of two parts which were the introduction chamber and analyzer.

Samples were introduced into the introduction chamber where a vacuum of 10^{-3} Torr was obtained using a Varian Vac-Sorb pump cooled by liquid nitrogen. Then the sample was inserted into the analyzer through a gate valve.

The analyzer contained the filament and the magnesium target. The photoejected electrons then pass into a nondisperseve electrostatic filter. This filter consists of two symmetric retarding fields.

The first retarding field encountered by the photoelectrons is used in the reflection mode and functions as a low energy pass filter. The second field is used in the transmission mode as a high pass filter. The first filter rejects high energy electrons by scattering from a solid plate which is the second field defining element of this filter. The second filter rejects low energy electrons by simple reflection. There is a small energy overlap between these two filters which yields a narrow transmission function. The resolution of this analyzer is dependent only upon the energy overlap of the two filters and the sharpness of their cut off characteristics and not on acceptance angle or apperture size. The electrons then pass into a electron multiplier. The pulse is sent to the electronics unit and the signal was plotted on a Hewlett Packard plotter on scaled graph paper. The user may determine the scale for both the X and Y asis. The binding energy could be set to any value up to about 1240 eV to within $\pm$ .1 eV. Binding energies were read from an Analogic digital meter. The vacuum, which was always $<10^{-7}$Torr was attained using a Perkin-Elmer ion pump.

Samples were introduced on a cylindrical brass probe. Samples were mounted on the flat surface perpendicular to the cylinder. The probe was mounted on a steel shaft which

was inserted as described previously.

Samples for both types of spectrometers were prepared in one of two ways:

1.) the sample was dusted on double stick tape on the probe.
2.) the sample was dispersed in acetone by ultrasonic agitation and by pipeting drops onto the surface of the brass probe.

The second method was used for all of the clay samples and for most of the standards. Only standards soluble in acetone or those that did not disperse well were put on the double stick tape.

When using the acetone dispersion technique, care was taken to get as thin a film as possible while still covering the entire probe surface. While using this technique, it was found that particle size was the main criterion for its success and ease of preparation. It was found that better films were achieved using smaller particles.

Calibration of the energy levels in both spectrometers was accomplished using the silicon 2p levels in clays as an internal reference and the carbon 1s level for all other materials. The carbon 1s level binding energy was 284.4 eV as determined by refering to the 4f $7/_2$ level of clean gold (binding energy 83.4 eV). For silicon 2p 1/2 levels, the absolute binding energy was 102.7 eV for kaolinite and 101.9 eV

for ripidolite as measured by referencing the carbon 1s level or to the $4f_{7/2}$ level of clean gold. For some samples where the metal hydroxide had obviously precipitated, the carbon 1s level and the gold $4f_{7/2}$ level were used as references.

The absolute binding energy of an element was determined by algebraic addition of the absolute binding energy of the reference element and the determined one. The charging correction or work function is then added or subtracted from the determined binding energy of the elements in question. The full width at half maximum (FWHM) is determined by measuring the width of the peak at a point midway between the peak maxima and a line drawn through the baseline of the peak.

G. Surface Area Measurements

The BET surface areas for the clays were measured in duplicate at liquid nitrogen temperature courtesy of Dr. J. P. Wightman. A typical sample weight of 0.500 grams clay was used in each surface area determination. The sample weights were measured on a Mettler type B-6 balance to the nearest 0.1 mg.. Nitrogen was used as the adsorbate gas. A FOCAL language computer program written by Dr. P. E. Field employed in conjunction with a PDP 8/I computer was used to calculate surface areas based on the BET equation. The specific surface areas of ripidolite and kaolinite are in Table III.

H. Cation Exchange Capacity Determination

Approximately 1.0 gram of the respective clay was weighed out and washed three successive times with 50 ml. portions of 0.2 N $MgCl_2$. After each 50 ml. addition of 0.2 N $MgCl_2$, the clay suspension was centrifuged. The clays were then washed with double distilled deionized water until the washings gave a negative test for Cl^- ion with the addition of silver nitrate solution.

About 0.05 grams of the Mg-saturated clay was then weighed out to the nearest 0.1 mg on a Mettler B-6 type balance. Two hundred mls. of 0.1N $BaCl_2$ was pipetted into the flask which contained the sample. The flasks were shaken for four hours and the resultant suspension was centrifuged until the supernatant appeared clear. Mg^{2+} content was determined by atomic absorption spectrophotometry. Standards were prepared from stock 0.1N $BaCl_2$ solution and a stock 1000 ppm Mg^{2+} solution. Cation exchange capacities were determined from a plot of meq/100g vs. the Mg^{2+} absorption reading for the standards. The specific cation exchange capacities are in Table III.

4. RESULTS AND DISCUSSION

A. Binding Energies of Lattice Elements

The binding energies for lattice elements in kaolinite had been determined previously in this laboratory and no attempt was made to confirm these values. The binding energies for ripidolite (a chlorite mineral) were determined by referencing the Si $2p_{1/2,3/2}$ level to the C 1s level and the Au $4f_{7/2}$ level and are listed in Table V. All other binding energies were calibrated using the Si $2p_{1/2,3/2}$ level and a minimum of three measurements of each was performed.

The binding energy for the Si $2p_{1/2,3/2}$ level of ripidolite is about 0.8 eV lower than that of the Si $2p_{1/2,3/2}$ level in kaolinite. This binding energy difference is greater than the difference between the oxygen binding energies or the aluminum binding energies in ripidolite and kaolinite. This greater difference in binding energies may in part be due to aluminum substituting for silicon in the tetrahedral layer of ripidolite while there is little or no substitution in the tetrahedral layer of kaolinite. Also, almost all of the cations in the octahedral layer are aluminum cations, while Fe^{2+}, Fe^{3+}, and Mg^{2+} are all substituted in the octahedral layer of ripidolite.

XPS is also capable of aiding in the examination of the oxidation state of iron. Koppelman[74] examined the oxidation state of Fe in several clay minerals. The binding

Table V

Core Electron Binding Energies and
FWHM for Mineral Lattice Elements (in eV ±.1)

	Ripidolite		Kaolinite[71]	
	B.E.	FWHM	B.E.	FWHM
Si $2p_{1/2,3/2}$	101.9	2.2	102.7	2.0
Al $2p_{1/2.3/2}$	74.3	2.6	74.4	2.1
O $1s_{1/2}$	531.3	2.4	531.9	2.4
Fe $2p_{3/2}$	711.3	6.7	———	———
Mg $2p_{1/2,3/2}$	49.7	1.8	———	———

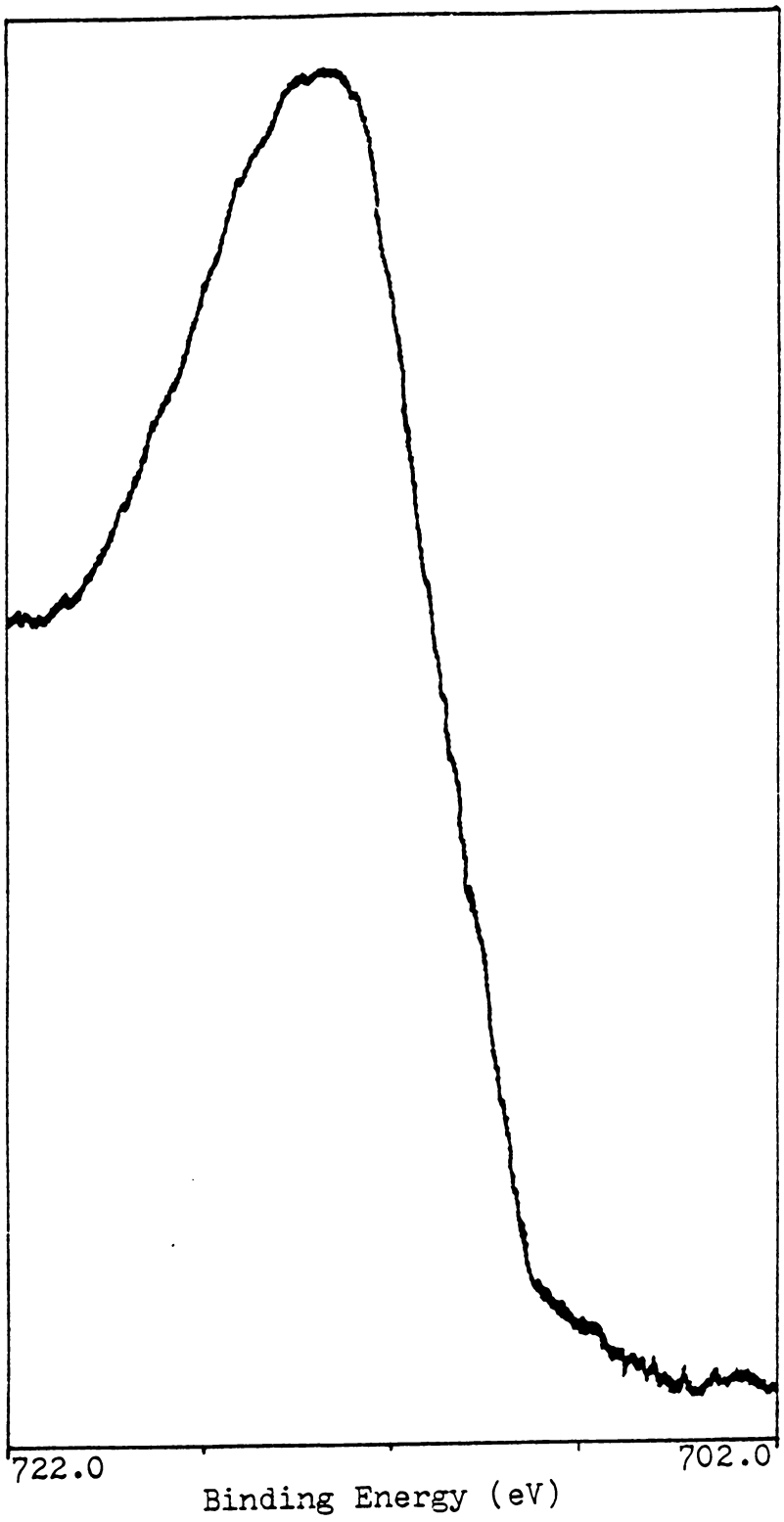

Figure 6. Fe $2p_{3/2}$ in ripidolite

energy of Fe $2p_{3/2}$ in chlorite was 710.6 eV and the iron was all ferrous as determined by Mossbauer spectroscopy. The Fe $2p_{3/2}$ binding energy of nontronite was determined to be 712.5 eV and was determined by Mossbauer spectroscopy to be all ferric in oxidation state. The Fe $2p_{3/2}$ binding energy of illite was 712.6 eV and the Fe in illite was determined to 82% ferric. The Fe $2p_{3/2}$ binding energy of ripidolite (Fig. 6) was determined to be 711.3 eV and the Fe in it was determined to be 84% ferrous and 16% ferric (Table I). Most of the Fe is ferrous so the binding energy tends toward that of Fe $2p_{3/2}$ in chlorite as expected. It can be concluded that although XPS can aid in the identification the Fe oxidation state, because there is only one peak, a ratio could not truly be determined.

Broadening of the Al, O, and Si photopeaks of ripidolite by about 0.4 eV ± 0.2 eV as compared to those of kaolinite was noted. This broadening is probably due to substitution of Al in the silicate tetrahedral layer and the varied cation environment in the octahedral layer of ripidolite.

Also the Al photopeak of ripidolite (Fig. 7A) is skewed to the low binding energy side, as compared to the Al photopeak of kaolinite (Fig. 7B). This may indicate the prescence of two or more Al photopeaks which overlap. Post et. al.[96] proposed a ratio of 1.36 Al to 2.64 Si in the tetrahedral layer with .85 Al to 5.24 of other elements in

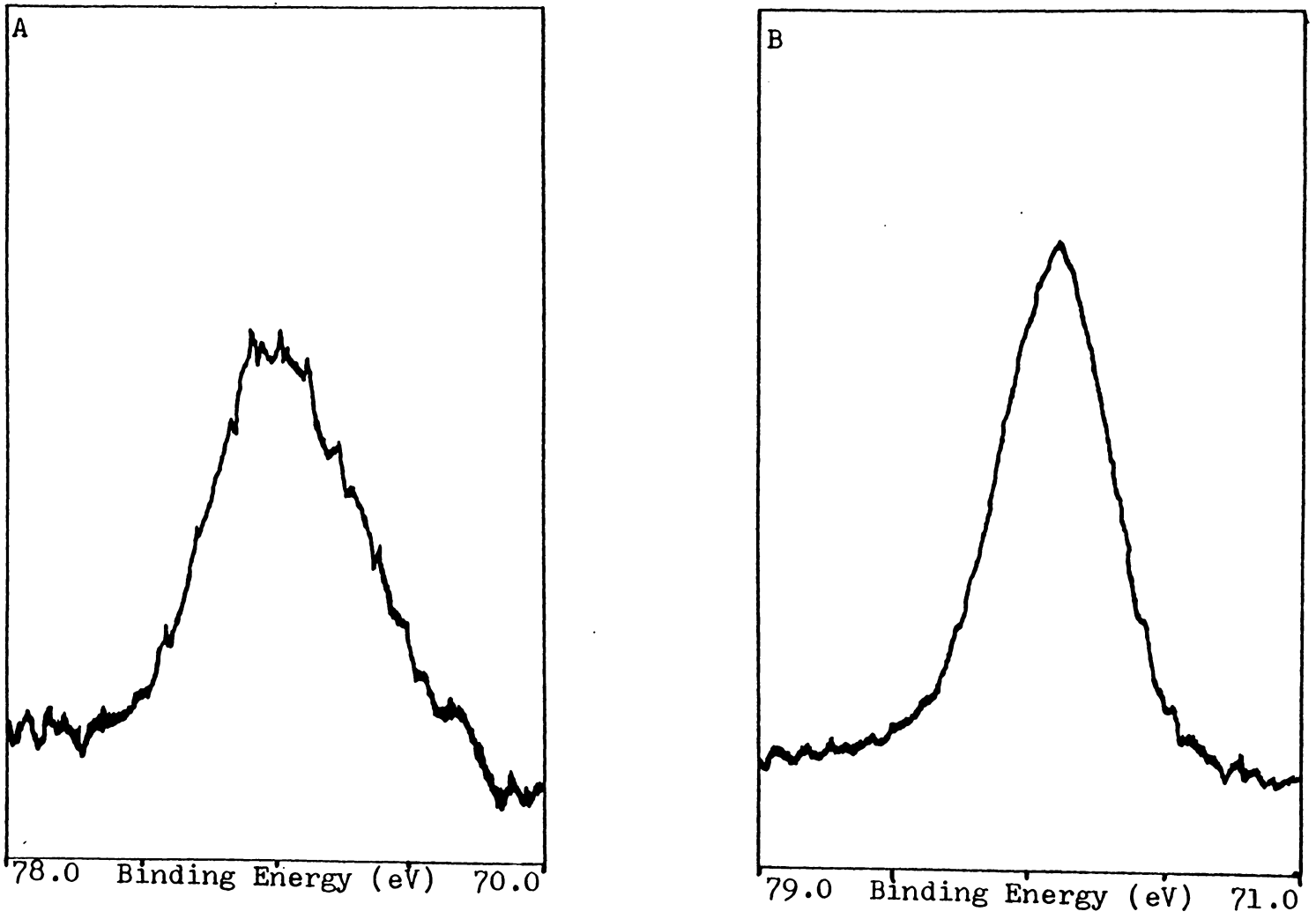

Figure 7. Al $2p_{1/2,3/2}$ for aluminum in ripidolite (A) and kaolinite (B)

Table VI

Comparison of Si, Al, and O Binding Energies of Silicates of Previous Investigators

Level	This Study	Koppelman[74]	Huntress[71] & Wilson	Adams[69] et al.	Schultz[72] et al.
		102.7 (Kaolinite)			109.3 Illite
		102.5 (Illite)	103 (avg)	102.2(avg.)	107.4 Kaolinite
Si $2p_{1/2,3/2}$	101.9 (Ripidolite)	102.1 (Chlorite)			
Al $2p_{1/2,3/2}$	74.3 (Ripidolite)	74.3 (avg.)	74 (avg.)	74.4 (avg.)	---------
O $1s_{1/2}$	531.3 (Ripidolite)	531.6 (avg.)	532 (avg.)	531.2 (avg.)	535 (avg.)

the octahedral layer. This represents a disproportionate ratio of 1.60 Al in the tetrahedral layer to 1.00 Al in the octahedral layer.

Anderson and Swartz[97] have attempted to correlate peak width and position of the Al 2p level with the coordination of Al in the three polymorphs, kyanite, sillimanite, and mullite. They concluded that the coordination number had no effect on either the peak position or width of the Al 2p level.

Koppelman[93] suggested that the greater number of positive cations in the crystal lattice of chlorite minerals as compared to kaolinite contributed to a lowering of the Si 2p level and Al 2p level in chlorite as compared to kaolinite. However, because no variety of minerals with different degrees of substitution were studied, no definite conclusion could be reached as to whether this hypothesis is true.

Binding energies of Si, O, and Al determined for ripidolite and those published by other researchers are in Table VI. The binding energies of all the elements are in close agreement with those of Huntress and Wilson[71] for various lunar and terrestial silicates, and those of Koppelman[74] for various silicate minerals. This is not unexpected, because the elements in question are both in the same chemical and geometrical environment. However, there is marked difference between the binding energies for Si and O

determined by other researchers and those observed by Schultz et al.[72]. This difference may be a result of a calibration problem due to insufficient or inadequate correction for charging by these authors.

B. The Determination of Al and Si Concentration on the Surface of Kaolinite

Recent efforts[86-89] have been made to determine the composition of the surface of solids quantitatively using XPS. Using XPS, the relative intensities of photopeaks are measured and corrected for differences in elemental photoionization cross-sections. The chief factors which contribute to the intensity of the XPS photopeak are, the mass absorption coefficient for the element, μ, the density of the solid sample, ρ, the intensity of the primary photobeam, I_0, and the depth in the sample of the particular element in question, τ.

Sieghbahn[54] proposed the following equation for the relative intensity, I, of an XPS photopeak;

$$I = I_0 e^{-\mu\rho\tau}$$

In order to relate intensities to percent composition, knowledge of the sampling depth is needed. This knowledge is not readily available, and usually all of the elements are considered to be at the same depth.

Coleman et. al.[98] determined that aluminum leached from H^+ clays in aqueous solution would be readsorbed on the

surface. In this study, an attempt was made to determine if the aluminum concentration on the surface did indeed change from that in the bulk. Also, it was of interest to see if the aluminum on the surface changed with changing pH. The kaolinite examined had been in aqueous solution for seven days at pH's 2, 4, 6, 8, and 10.

The photoionization cross-section relative to carbon 1s for silicon $2p_{1/2,3/2}$ and aluminum $2p_{1/2,3/2}$ levels taken from Scofield[99] are 0.866 and 0.574 respectively. Elemental composition analysis were reported relative to the silicon abundance in the sample. The experimental values for these ratios were calculated from the following formulas:

$$Si/Al = RI_{SI}/RI_{AL}$$

where relative intensity (RI) photopeak =

(net XPS counts for photopeak) x (height of photopeak) x FWHM/(photoionization cross-section for particular elements photopeak)

The results are in Table VII. Error in the measurements of the peak are about 2-3%. The data demonstrates that more Al is on the surface of the clay at low pH than the bulk composition ratio would indicate. Further, as the pH increases, less aluminum is leached from the clay and readsorbed on the surface. This is inferred from the fact that the Al/Si ratio of the untreated clay is

Table VII

XPS Al/Si Ratio of Treated
and Untreated Samples of Kaolinite

Sample	Al/Si
Bulk Analysis as analyzed by chemical analysis	0.85
Untreated kaolinite determined by XPS	0.85±.02
Kaolinite treated at	
pH 2	0.95±.01
pH 4	0.93±.02
pH 6	0.92±.02
pH 8	0.89±.02
pH 10	0.87±.02

the same as the bulk composition ratio.

In Tables VIII and XIII the aluminum concentration is about equal to that of silicon in solution in acidic media, at higher pH values, neither appears to have undergone any dissolution. This, together with the XPS data, indicate that the aluminum leached from the surface at low pH is probably preferentially readsorbed onto the clay surface.

C. Adsorption of Cobalt on Ripidolite and Kaolinite

Previous studies[73-75] have demonstrated the applicability of XPS to the study of adsorbed metal ions and complexes on a substrate. In this study, Co^{2+} was one of two divalent cations whose adsorption on kaolinite and ripidolite was studied. Co^{2+} was chosen because the species in solution at different pH values were well characterized. The objectives of this study were to examine what effect pH had on cation adsorption and to explore the suggestion by Tewari and Lee[47] that in the pH range 6-8, cobalt precipitates as a hydroxide species on the adsorbent surface. In their case, various metal oxides were used.

Adsorption experiments were performed at pH 2, 4, 6, 7, 8, and 10. The solution concentration data for these experiments appears in Tables VIII and IX.

The amount of Co^{2+} adsorbed at pH 2 and 4 by 2.5 grams of either clay was neglible. The amount of Co^{2+} adsorbed on kaolinite and ripidolite at pH 6, 7, 8, and 10

Table VIII

Cobalt Adsorption on Kaolinite at pH 2, 4, 6, 7, 8, 10

	pH 2		pH 4		pH 6		pH 7		pH 8		pH 10	
Max. pH	2.05		4.08		6.68		7.47		8.04		10.10	
Min. pH	1.92		3.99		5.70		6.59		7.08		9.97	
Avg. pH	1.98±.01		4.05±.02		6.03±.20		6.97±.15		7.77±.09		10.05±.02	
Species Analyzed	I	F	I	F	I	F	I	F	I	F	I	F
SiO_2	0	1	0	0	0	1	0	1	0	1	0	0
Co	101	100	100	100	100	98	100	92	101	76	3	0
Fe	0	0	0	0	0	0	0	0	0	0	0	0
Mg	1	5	1	4	2	4	2	4	1	4	1	5
K	0	0	0	0	0	0	0	0	0	1	0	1
Al	0	2	0	1	0	0	0	0	0	0	0	0

I is equal to Initial
F is equal to Final

Table IX

Cobalt Adsorption on Ripidolite at pH 2, 4, 6, 7, 8, and 10

	pH 2		pH 4		pH 6		pH 7		pH 8		pH 10	
Max. pH	2.10		4.27		6.25		7.12		8.20		10.10	
Min. pH	1.96		3.96		5.35		6.33		7.05		9.98	
Avg. pH	2.02±.02		4.09±.06		6.02±.13		6.82±.17		7.76±.16		10.07±.02	
Species Analyzed	I	F	I	F	I	F	I	F	I	F	I	F
SiO_2	0	5	0	4	0	2	0	3	0	1	0	1
Co	100	100	101	100	100	97	100	94	100	87	0	0
Fe	0	9	0	2	0	0	0	0	0	0	0	0
Mg	0	43	0	34	0	21	2	21	1	18	1	4
K	0	0	0	0	0	0	0	0	0	0	0	1
Al	0	9	0	3	0	0	0	1	0	0	0	0

I is equal to Initial
F is equal to Final

Table X

Cobalt Adsorption by Ripidolite and Kaolinite at pH 2, 4, 6, 7, 8, 10

pH of Sample	Amt. Co^{2+} adsorbed on Ripidolite (meq/100 gms)	Amt. Co^{2+} adsorbed on Kaolinite (meq/100 gms)
6	2.0	1.3
7	4.1	5.4
8	8.8	17.0
10	67.9	67.9

is in Table X. The amount of Co^{2+} adsorbed is expressed in the same terms as CEC which is milliequivalents per 100 gms of clay.

From the three tables, two obvious facts appear. First, as pH increases, the dissolution of elements, particularly magnesium, decreases. Second, as pH increases, the adsorption of Co^{2+} also increases until precipitation of Co^{2+} as some cobalt hydroxy compound begins at pH 8. At pH 10, the cobalt had formed a visible precipitate before being mixed with the clay.

The only species present in solution at pH 2 and pH 4 is $Co(H_2O)_6^{2+}$. At pH 6 and pH 7, $Co(H_2O)_6^{2+}$ represents 99.9% and 99.4% of the species of Co^{2+} present in solution, respectively. The only other species at these pH values is $Co(OH)(H_2O)_5^{+}$ and it represents 0.1% and 0.6% respectively of the amount of cobalt present at pH 6 and pH 7. It is apparent that the $Co(H_2O)_6^{2+}$ concentration is several orders of magnitude greater than that of $Co(OH)(H_2O)_5^{+}$. Therefore, any adsorption of the $Co(OH)(H_2O)_5^{+}$ ion would probably be masked by the adsorption of the $Co(H_2O)_6^{2+}$ ion at those pH values. At pH 8, the precipitation of $Co(OH)_2$ has just begun and $Co(OH)(H_2O)_5^{+}$ represents about 4.5% of the solution. At pH 10 most of the cobalt has precipitated as $Co(OH)_2$, while less than 0.001% remains as $Co(H_2O)_6^{2+}$ and $Co(OH)(H_2O)_6^{+}$ in solution. Therefore, at pH 8 and pH 10, the hydroxy forms of Co^{2+} may play an important role, and

the precipitation and/or adsorption of Co^{2+} hydroxy species at pH 8 may account for the apparent increased adsorption of Co^{2+}. From the solution data alone, however, one could not truly deduce how the Co^{2+} is associated with the clay.

The cobalt $2p_{3/2}$ binding energies for $Co(OH)_2$, CoO, CoOOH, Co_3O_4, $Co(NO_3)_2 \cdot 6H_2O$ and cobalt adsorbed on ripidolite and kaolinite at pH's 2, 4, 6, 7, 8, and 10 were measured and are presented in Table XI.

The binding energies of Co $2p_{3/2}$ determined in this study were compared to those of other investigators in the literature. Correction for differences in calibration procedure was made where needed for the literature binding energies. The Co $2p_{3/2}$ binding energies of Co_2O_3 and Co_3O_4 agreed closely with those of Burness[100]; and the Co $2p_{3/2}$ binding energies of $Co(NO_3)_2 \cdot 6H_2O$ and $Co(OH)_2$ agreed closely with those of Koppelman.[93]

However, none of the Co $2p_{3/2}$ binding energies determined by other investigators[82,101,102] compared favorably with each other or the ones determined by this investigator. This points out the continued problem of inter lab calibration with XPS binding energies when no binding energy for an internal calibrant exists. The binding energies of Koppelman[93] and Burness[100] were determined in the same lab as this investigator, and the same binding energy for the external calibrants were used. But by comparison, no agreement among the several investigator's labs is apparent.

Table XI
Cobalt Binding Energies (Co $2p_{3/2}$ level)

Compound	Binding Energy	FWHM	Satellite Intensity	Co $2p_{1/2}$-$3/2$
Lusakite	782.6±0.3[93]	5.4	-	15.7
$Co(OH)_2$	780.8,781.1[101],780.4[102]	4.2	S	16.0
CoO	780.4,781.1[101],779.4[82]	4.8	M	15.5
$Co(NO_3)_2.6H_2O$	781.7,781.6[93]	5.1	S	
Co_3O_4	779.8,779.5[100],780.3[101]	3.4	W	
CoOOH	780.1,779.4[82]	2.7	W	
Co_2O_3	779.3,779.4[100]	3.3	W	
Cobalt Adsorbed on Kaolinite				
pH 2	783.2		M-S	--
4	783.1			14.7
6	782.8		M-S	14.9
7	782.8	5.6	S	14.8
8	781.2	4.5	S	15.6
10	781.0	4.5	S	15.6
Cobalt Adsorbed on Ripidolite				
pH 2	782.1			15.1
4	782.0			15.2
6	781.6		M-S	15.8
7	781.1	4.6	S	15.9
8	781.1	4.4	S	15.8
10	781.0	4.3	S	15.8

Therefore, it appears that when one discusses binding energy data determined in the investigators own lab in comparison with literature values that differences result from disagreement on a binding energy of an external reference.

In examining the spectra of adsorbed cobalt on kaolinite and ripidolite, three questions may be asked. First, what is the chemical nature of the adsorbed cobalt on the clay? Second, is it possible to identify what species of cobalt, i.e., $Co(OH)_2$ is associated with the surface of the clay? Third, can the spectra of adsorbed cobalt show how the cation is bound to the surface?

Frost[67] et. al. in a study of a number of cobalt compounds found that the oxidation state of cobalt could not be assigned from binding energy data. Because of changes in the spin states of both Co^{2+} and Co^{3+}, the binding energies overlap. Instead, the intensity of satellites which occur at a higher binding energy than the main photopeak are used to determine the oxidation state. Co^{2+} (high spin) spectra have intense satellite structure while those of Co^{3+} (low spin) have very weak satellite structure.

For the purpose of this thesis, a relative assignment of satellite intensity was made for each spectrum of cobalt adsorbed on both kaolinite and ripidolite. Those spectra with satellites of intensity similar to that of $Co(OH)_2$

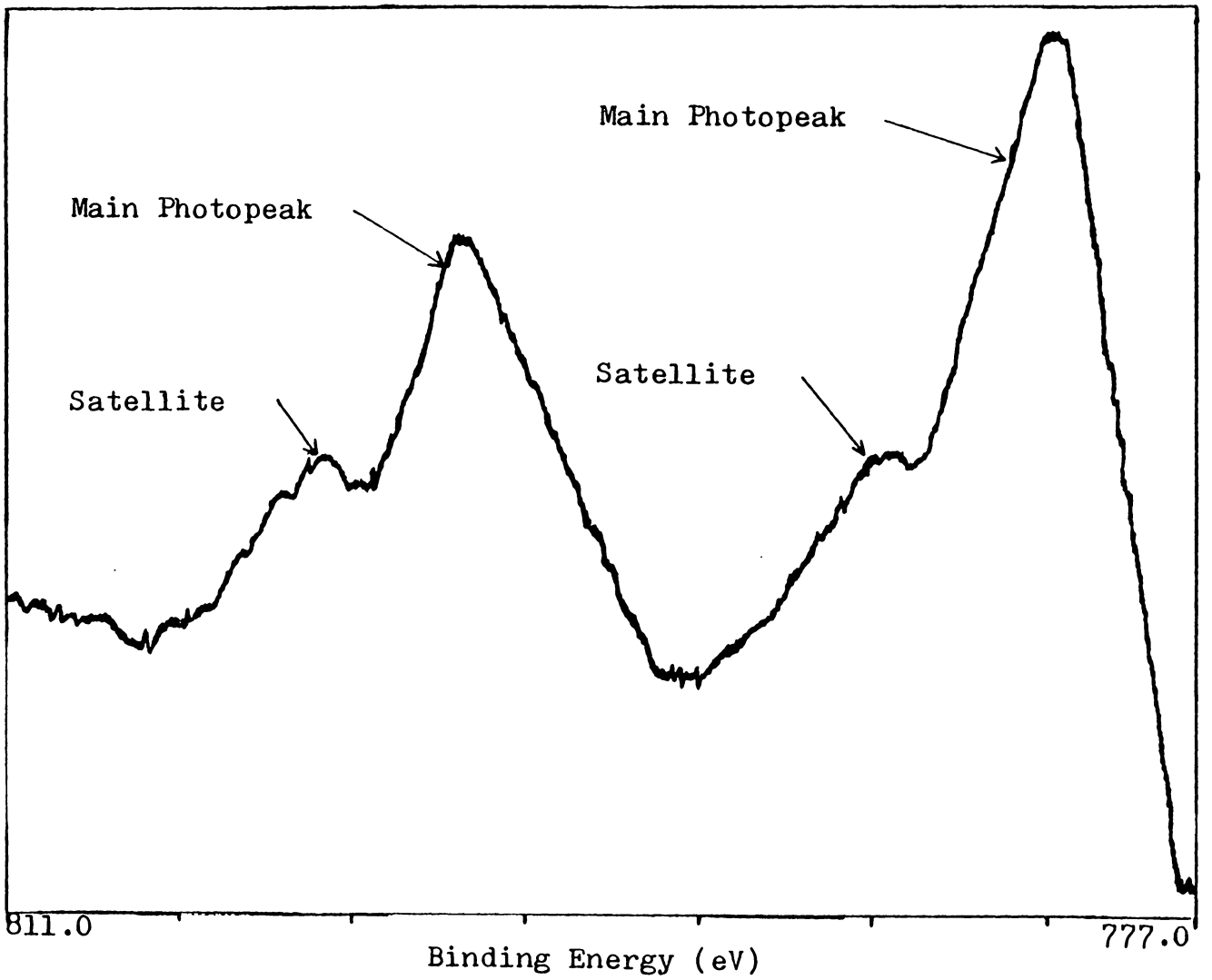

Figure 8. Co $2p_{1/2,3/2}$ in $Co(OH)_2$

(high spin Co^{2+}) Fig. 8 are marked with an S for strong intensity in Table XI. Those with medium intensity satellites similar to that of CoO (high spin Co^{2+}) Fig. 9 are marked with an M for medium intensity. Those with weak or no satellite such as CoOOH (low spin Co^{3+}) Fig. 10 are marked with a W for weak or no intensity of satellite peaks in Table XI.

For cobalt adsorbed on ripidolite and kaolinite at pH 7, 8, and 10, the Co $2p_{3/2}$ satellites were of strong intensity. This is strong evidence that the Co^{2+} which had been in the solution had remained Co^{2+} when it had become associated with the surface of the clay.

The Co $2p_{3/2}$ photopeaks that were determined for cobalt adsorbed on kaolinite and ripidolite at pH 2, 4, 6, and 7 were of weak intensity. However, satellites were apparent and when comparison was made, the satellites were of medium to strong intensity indicating that Co^{2+} is on the surface of the clay also.

In order to answer the second question of what species of Co^{2+} is adsorbed at the various pH values, several factors must be taken into account. These factors are important because they help to identify the spin state and/or the covalency of the bond as well as helping to more thoroughly confirm the identification of the peaks in question. In order to make a valid comparison between the peaks of pure compounds and that of the adsorbed species,

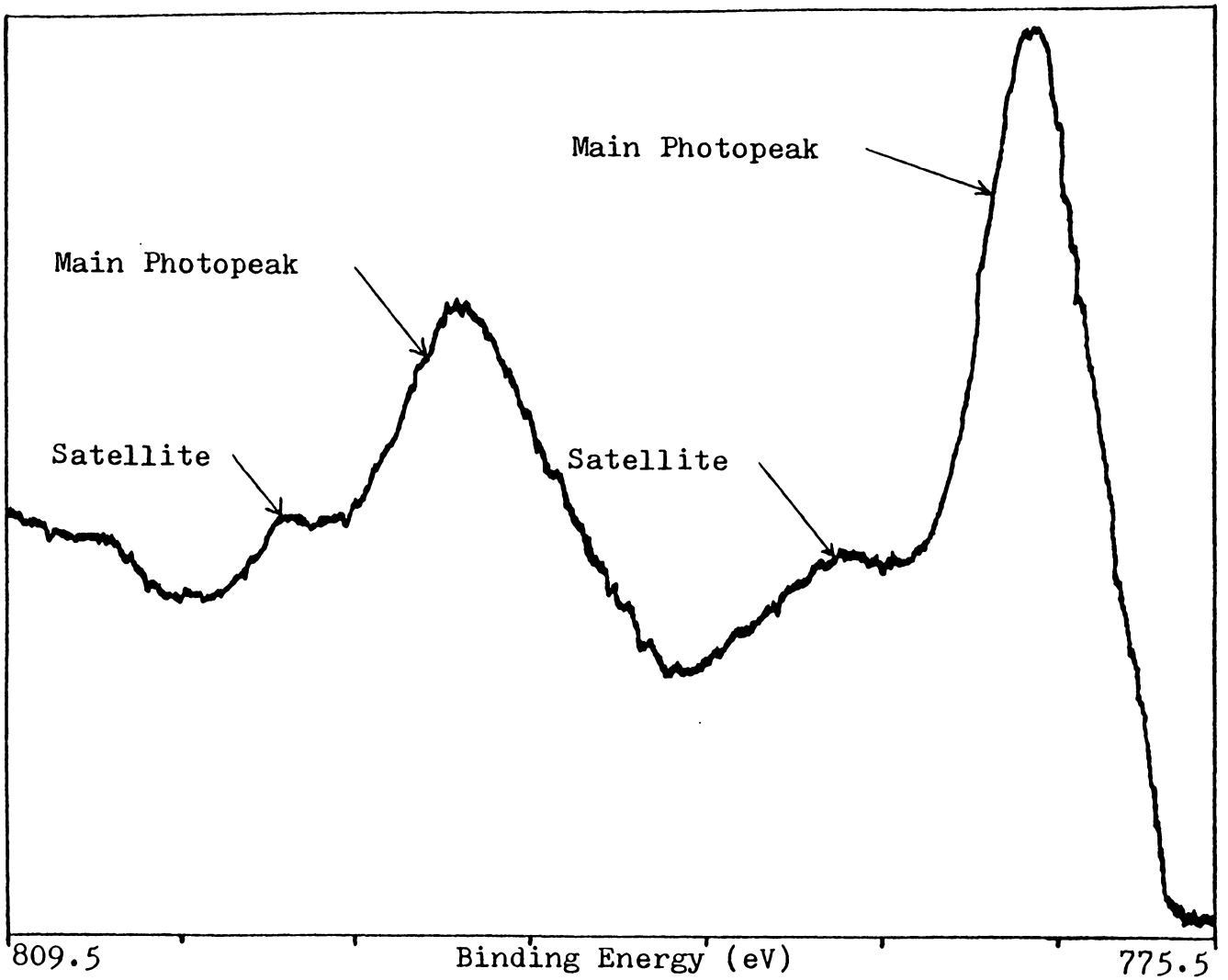

Figure 9. Co $2p_{1/2,3/2}$ in CoO

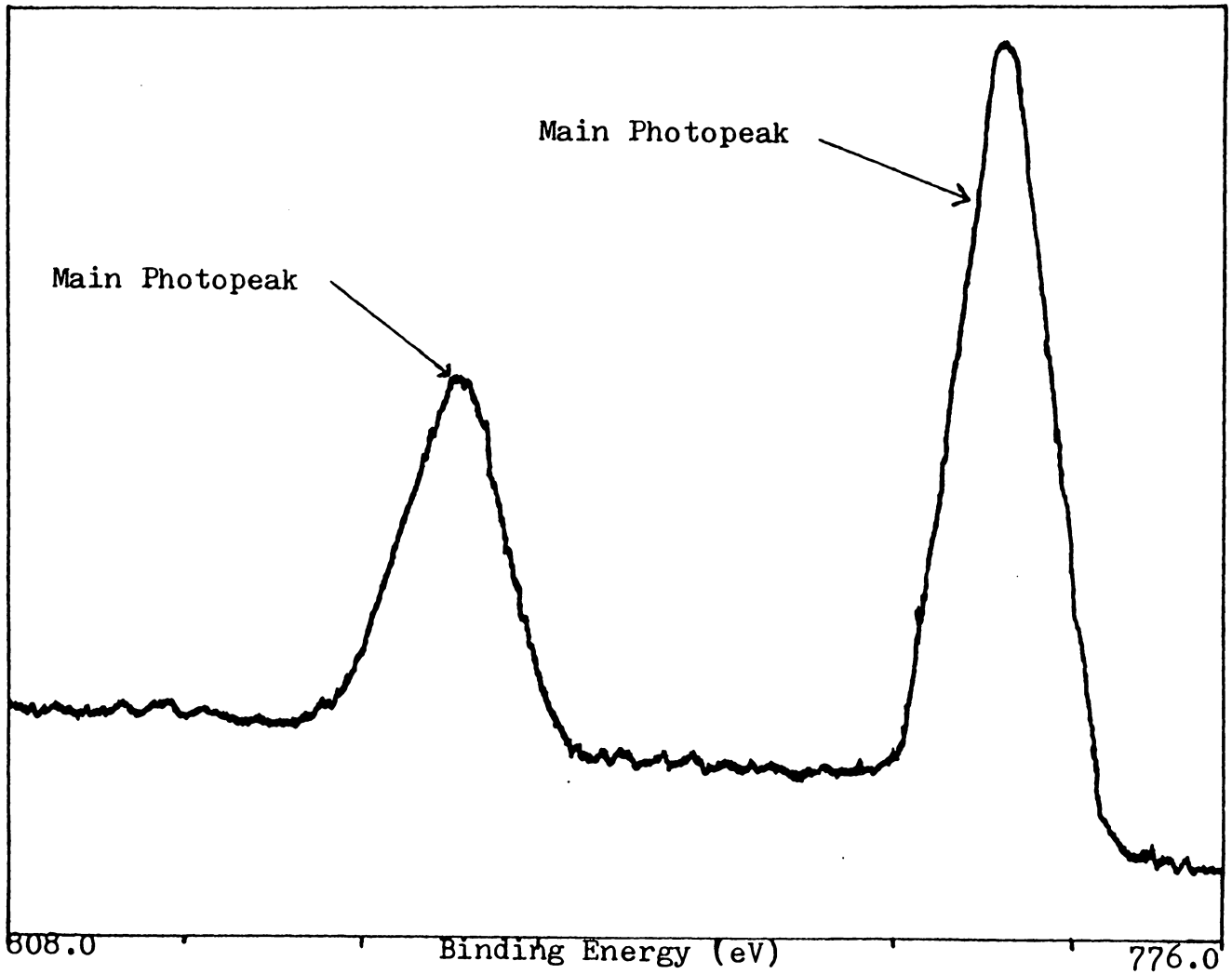

Figure 10. Co $2p_{1/2,3/2}$ in CoOOH

three factors must be known.

One should know the FWHM (Full Width at Half Maximum) of the main photopeak, the satellite intensity and the Co $2p_{1/2}$-Co $2p_{3/2}$ splitting. If each of these factors is the same for both the compound and the adsorbed element in question, then a comparison of the binding energies can be made. The data for each of these factors are listed in Table XI along with binding energy values of the standard reference compounds and for cobalt adsorbed on the clays at the various pH values.

First, it must be stated that at pH 10, a cobalt hydroxy precipitate had formed before the clay was mixed with the solution. It would be expected that the Co $2p_{3/2}$ spectra of $Co(OH)_2$ would closely resemble that of the cobalt at pH 10 on ripidolite and kaolinite. As expected the binding energies are within experimental error of each other as are the Co $2p_{1/2}$-Co $2p_{3/2}$ splittings and the satellite intensities. The Co $2p_{3/2}$ photopeak of kaolinite at pH 10 is slightly broader than that of $Co(OH)_2$, but it is also within the limits of precision (±.2 eV). Therefore, at pH 10, the species of Co^{2+} associated with either clay is similar to or is $Co(OH)_2$.

At pH 8, the question of what species is present becomes more clouded. At pH 8, the solution is on the borderline of precipitation of $Co(OH)_2$. It was at this pH, that a dramatic increase in the uptake of Co^{2+} was noted.

This would be expected, however if partial precipitation of a cobalt hydroxy species had occurred. Throughout the experiment, the control had not shown any signs of a precipitate being formed. The Co $2p_{3/2}$ peak of cobalt adsorbed on ripidolite at pH 8 is similar in every respect to those of cobalt adsorbed at pH 10 and to that of $Co(OH)_2$. Therefore, it is likely that $Co(OH)_2$ or some cobalt hydroxy compound has precipitated on the surface at pH 8. In this way, the clay would behave as a nucleation center for the formation of the hydroxides of cobalt.

The Co $2p_{3/2}$ peak of cobalt adsorbed on kaolinite at pH 8 is similar to that of cobalt adsorbed at pH 10 and $Co(OH)_2$. This seems to indicate that $Co(OH)_2$ or some cobalt hydroxy species is most likely associated with the kaolinite surface at this pH and that this clay also behaves as a nucleation center for the formation of cobalt hydorxide species on its surface.

The Co^{2+} species adsorbed on either clay at pH 2, 4, 6, and 7 cannot be determined from the present XPS spectra examined. Each clay will be discussed separately.

The cobalt adsorbed on ripidolite at pH 7 had a Co $2p_{3/2}$ binding energy of 781.1 eV and a Co $2p_{1/2}$-Co $2p_{3/2}$ split of 15.9 eV. Frost et. al.[67] determined that the Co $2p_{1/2}$-Co $2p_{3/2}$ splitting usually changes with a change in spin state. Specifically that Co^{2+} high spin has a splitting of approximately 16.0 eV while Co^{2+} low spin and

Co^{3+} low spin have a splitting of about 14.9 eV. Also the Co $2p_{1/2}$-Co $2p_{3/2}$ splitting of some Co^{2+} compounds has been shown to be due to covalency, with a splitting as low as about 15.0 eV for $Co^{II}S$ where the Co^{2+} is known to be high spin. Therefore, it is concluded that Co^{2+} adsorbed at pH 7 on ripidolite is high spin Co^{2+}. The satellite was of the same intensity as those of cobalt adsorbed on ripidolite at pH 8 and 10.

This evidence indicates that the same species of cobalt is associated with the clay as that at pH 8 and 10. If this is true, it would mean that a cobalt hydroxy species had precipitated at a pH significantly below that of the precipitation of cobalt hydroxide. However, no significant increase in the removal of Co^{2+} from solution occurred between pH 6 and pH 7 as it did between pH 7 and pH 8. Therefore, it cannot be conclusively stated that the Co^{2+} adsorbed at pH 7 is a cobalt hydroxy species.

The Co^{2+} adsorbed on ripidolite at pH 6 has a binding energy of 781.6 eV and a Co $2p_{1/2}$-Co $2p_{3/2}$ splitting of 15.9 eV. The Co $2p_{3/2}$ satellite is of strong intensity indicating that at high spin Co^{2+} is the chemical nature of the cobalt on the surface. The Co $2p_{3/2}$ binding energy is about 0.5 eV higher than that for Co^{2+} adsorbed on ripidolite at pH 7. This may indicate that a different species of cobalt has been adsorbed, possibly $Co(OH)(H_2O)_5^+$ or $Co(H_2O)_6^{2+}$. It must be remembered that the removal of electron density

from an atom causes the binding energy to go up. Therefore it could be concluded that the OH^- group is donating more electron density to the Co^{2+} than the clay surface.

At pH 4, the Co^{2+} adsorbed on ripidolite has a binding energy of 782.0 eV and a Co $2p_{1/2}$-Co $2p_{3/2}$ split of 15.2 eV. The Co $2p_{3/2}$ binding energy has increased 0.4 eV relative to pH 6. Also the Co^{2+} is either low spin or the bond is of a highly covalent nature. This indicates yet another species change on the surface. These changes in the Co $2p_{3/2}$ binding energy may also indicate a change on the surface of the clay such as changing charge density or different adsorption sites. A study of the adsorption of other cations might help demonstrate which effect is taking place.

The Co $2p_{3/2}$ binding energy of Co^{2+} adsorbed on ripidolite at pH 2 is equal to that at pH 4 and the Co $2p_{1/2}$-Co $2p_{3/2}$ splitting is 15.1 eV. The satellite is of strong intensity, indicating the presence of Co^{2+}. Therefore, at pH 2, the adsorbed cobalt on ripidolite is either low spin Co^{2+} or the bond is of a highly covalent nature. The use of UV-visible or electron spin resonanace spectroscopy could aid in determining the spin state of the adsorbed Co^{2+}.

The Co^{2+} adsorbed on kaolinite at pH's 2, 4, 6, and 7 had similar Co $2p_{3/2}$ binding energies, Co $2p_{1/2}$-Co $2p_{3/2}$ splittings and satellite intensities. In all cases the Co $2p_{3/2}$ binding energy was 783.0±0.2 eV, the Co $2p_{1/2}$-Co $2p_{3/2}$ splitting was 14.8±0.1 eV and the satellite was of medium to

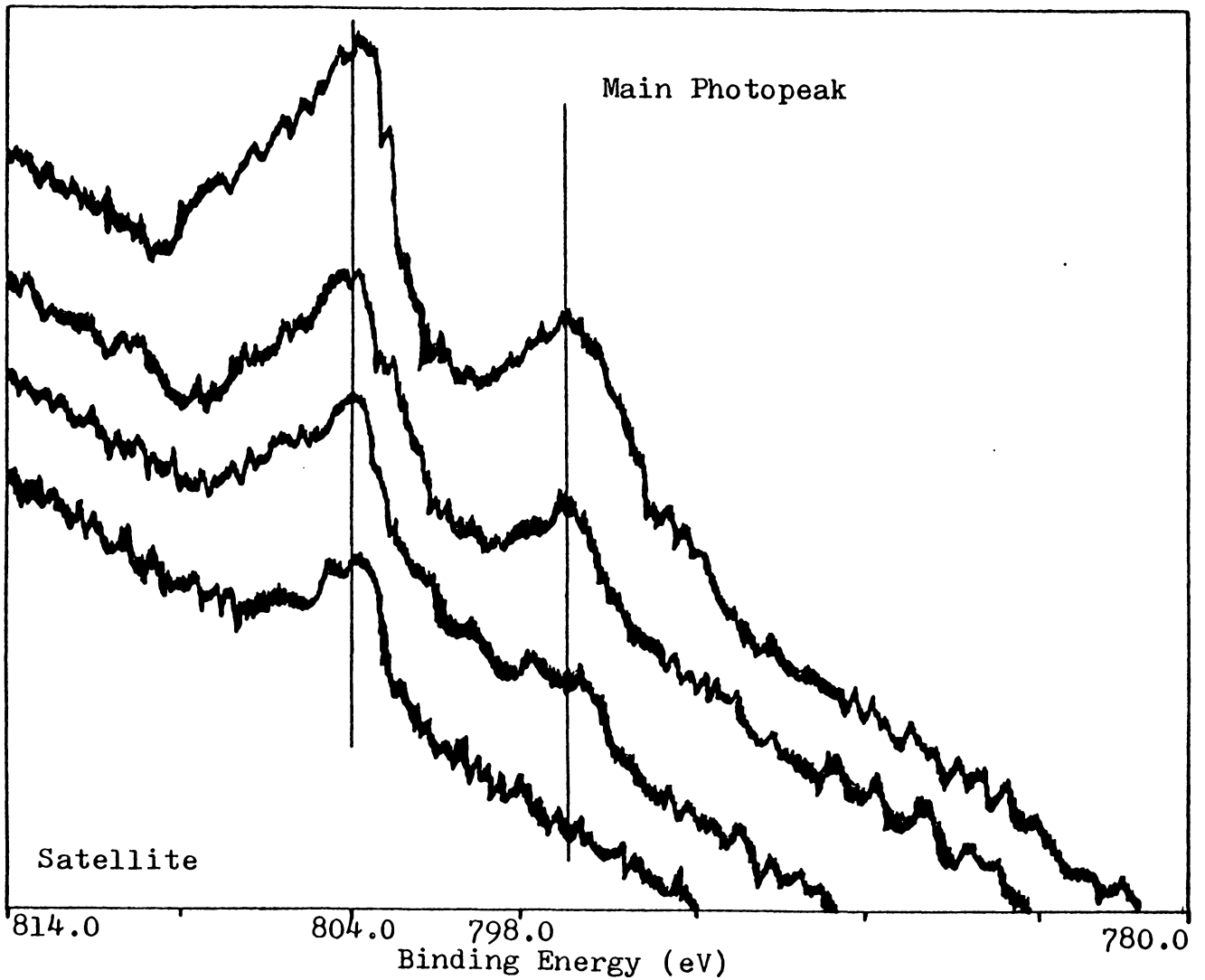

Figure 11. Co $2p_{1/2}$ of Co^{2+} adsorbed on kaolinite at pH 2,4,6, and 7

strong intensity. This was not like ripidolite over the same pH range where the binding energy changes at each pH value.

Although the exact nature of the Co^{2+} species adsorbed on kaolinite cannot be ascertained, the nature of the cobalt to clay bond can be discussed. The Co^{2+} is either low spin or else the bond is of a highly covalent nature. In either case, this indicates the formation of a covalent bond on the surface of the clay between the Co^{2+} and the adsorption site.

Also, when one examines the Co $2p_{1/2}$ peak, the satellite is found to be of greater intensity than the main photopeak. As the pH decreases towards 2, the satellite intensity continues to increase, while that of the main photopeak decreases (Fig. 11). As was stated earlier, satellites are due to several processes of which the main two are "shake-up" processes and multiplet splitting. Frost[67] states that the satellite intensity due to "shake-up" processes is constant while that of multiplet splitting varies according to the amount of charge transfer between it and the donating ligand. The greater the charge transfer between the ligand and the cation, the greater the contribution to the satellite intensity. This implies that as the pH decreases, the amount of the charge transfer increases. The same decrease in intensity of the main photopeak and increase in satellite intensity for the Co $2p_{1/2}$ peak for Co^{2+} adsorbed on ripidolite at pH 2, 4, and 6

occurs also.

The Co $2p_{3/2}$ binding energy, for Co^{2+} adsorbed on kaolinite below pH 7 is 0.4 eV higher than that for Co^{2+} in lusakite. This raises the question as to whether the Co^{2+} adsorbed on kaolinite is adsorbed or whether it has penetrated to the octahedral site of kaolinite. The Co $2p_{1/2}$-Co $2p_{3/2}$ splitting of Co^{2+} in lusakite is 15.7 eV indicating that the Co^{2+} is high spin. This demonstrates that the Co^{2+} at pH 2, 4, 6, and 7 on kaolinite, and at pH 2 and 4 on ripidolite is not lattice substituted, but actually is adsorbed.

The high Co $2p_{3/2}$ binding energy value of Co^{2+} adsorbed on kaolinite is probably indicative of the charge transfer from the cobalt ion to the clay surface. As charge is transfered from the cobalt ion, the cobalt binding energy would increase.

Besides obtaining binding energy data from the spectra, one can also extract semi-quantitative data on the amount of an element present on the surface in comparison to another. This was done for cobalt using the expression:

$$Co/Si = RI_{Co}/RI_{Si}$$

where RI_{Co} stands for the relative intensity of the cobalt peak calculation from a photoionization cross-section of 12.40 [99] and RI_{Si} represents the relative intensity of the silicon peak.

Table XII

Co/Si Ratio for Cobalt Adsorbed on Kaolinite and Ripidolite

pH	Co/Si Ratio for Co^{2+} Adsorbed on Kaolinite ($x10^4$)	Co/Si Ratio for Co^{2+} Adsorbed on Ripidolite ($x10^2$)
6	9.2	3.4
7	17.5	5.6
8	147	20
10	714	111

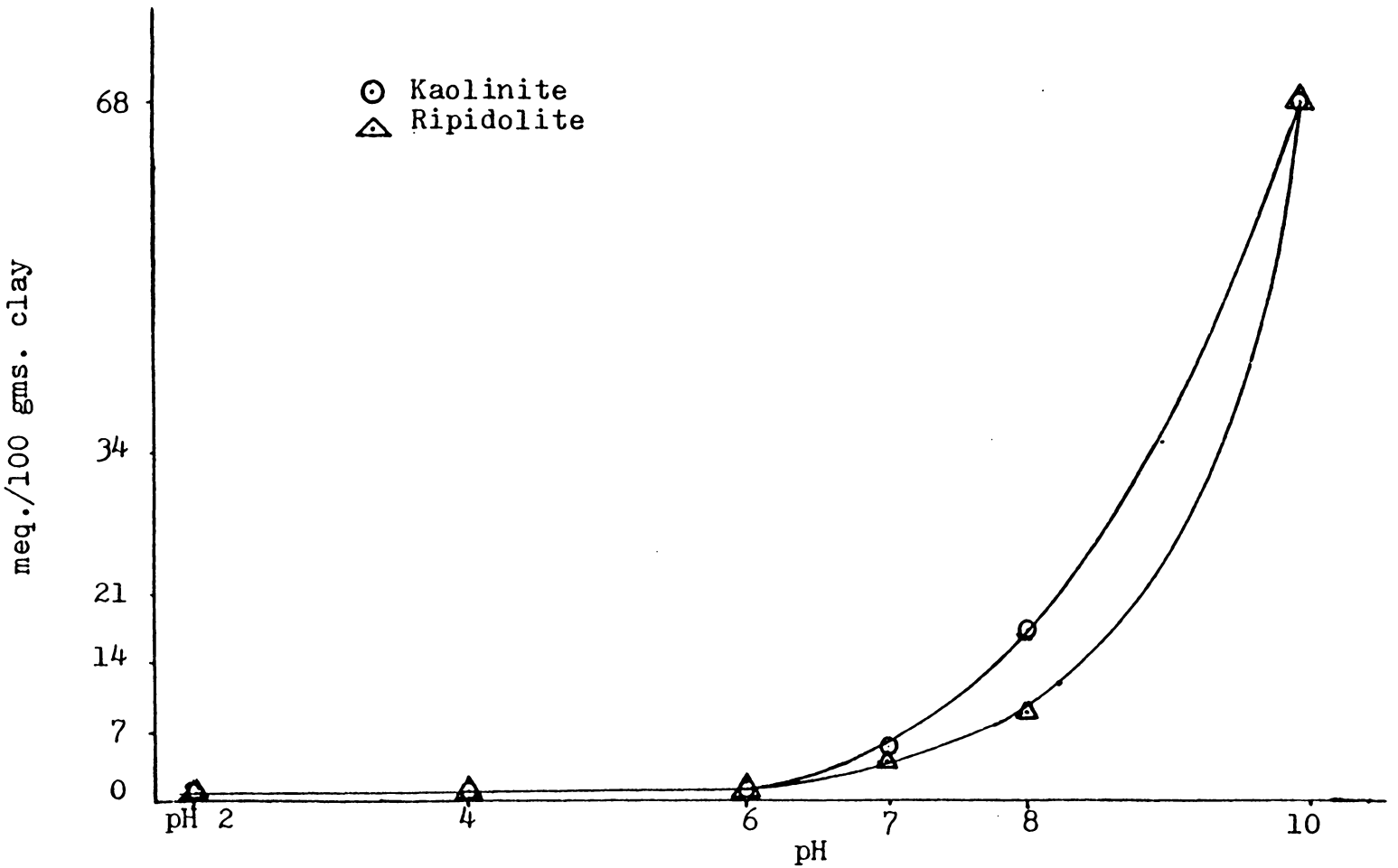

Figure 12. Uptake of Co^{2+} by ripidolite and kaolinite

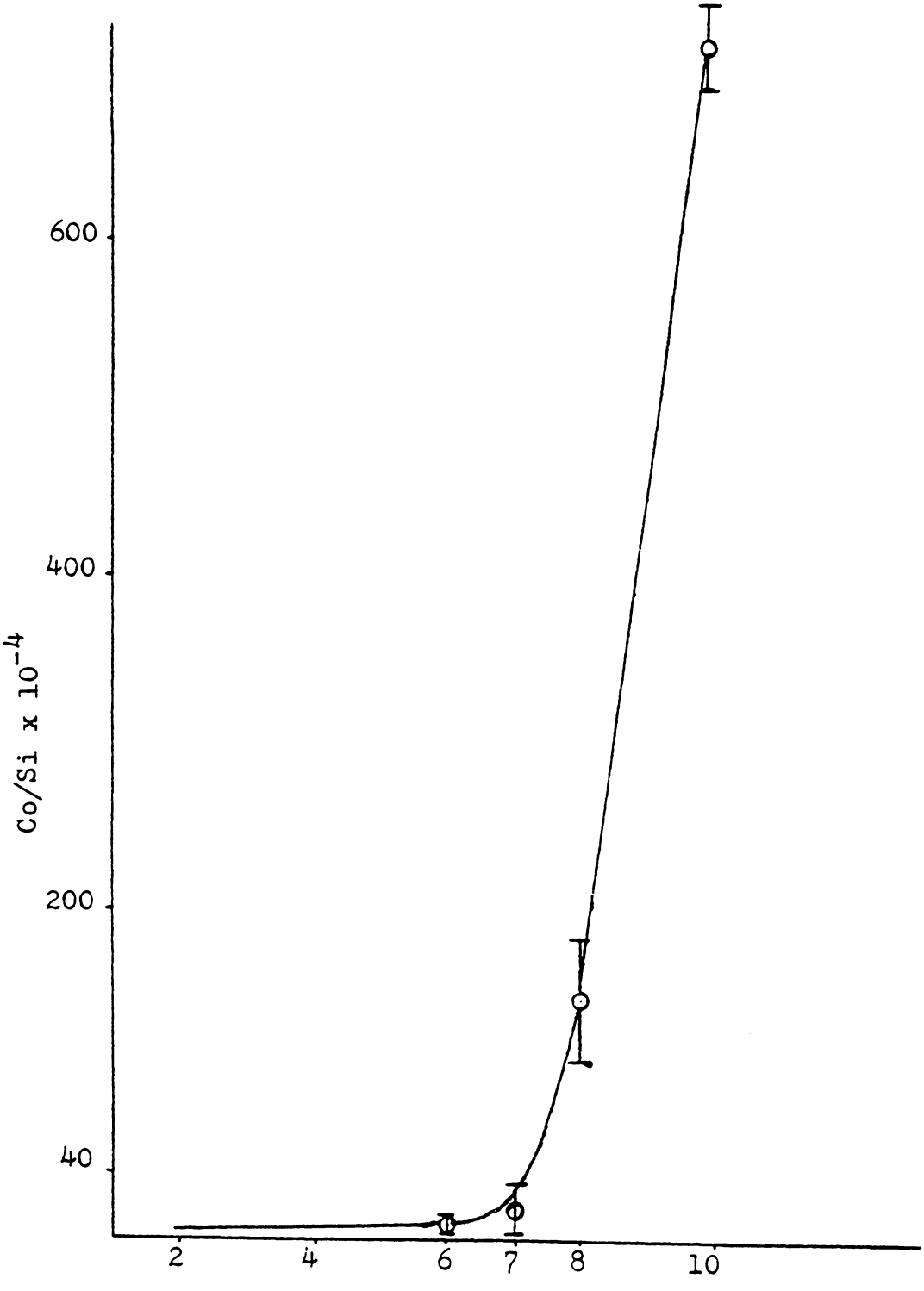

Figure 13. Uptake of Co^{2+} by kaolinite

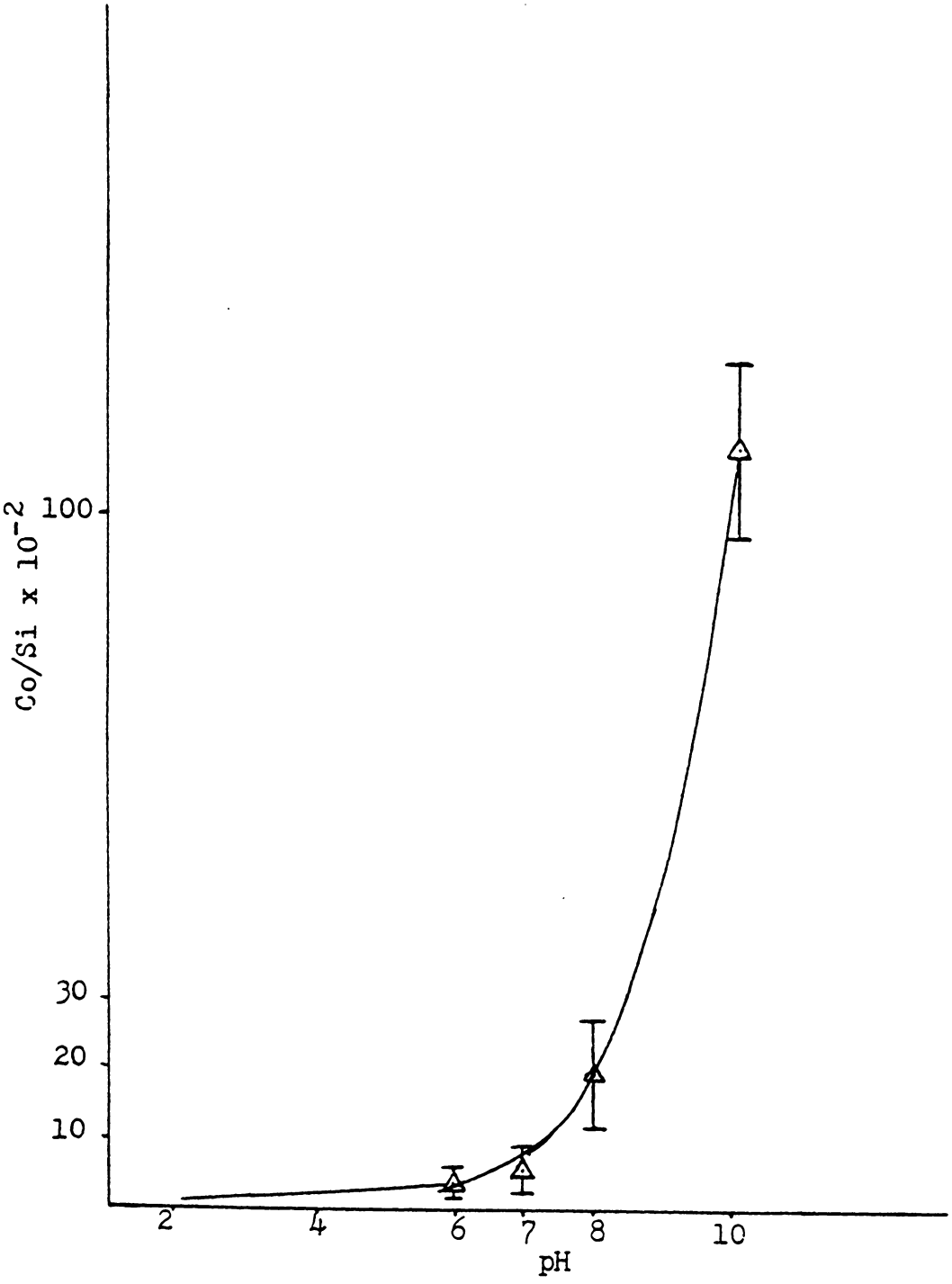

Figure 14. Uptake of Co^{2+} by ripidolite

The cobalt to silicon ratios calculated for the cobalt adsorbed on kaolinite and ripidolite are in Table XII and plotted against the pH at which adsorption took place in Figures 11 and 12. And in Figure 13 the amount of cobalt removed from solution, which was determined by atomic absorption spectroscopy, is also plotted against the pH at which removal took place. The concentrations for these plots were taken from solution data in Tables VIII and IX. Figures 12, 13, and 14 all show good agreement, especially as to shape and trend. All three plots show an increased removal of Co^{2+} from solution or of Co^{2+} being associated with the clay surface as the solution pH increases.

D. Adsorption of Cr^{3+} on Kaolinite and Ripidolite

Having investigated the adsorption of the divalent cation Co^{2+}, a study of Cr^{3+}, was performed. Chromium was chosen because the species in solution at various pH's are known and because it also had an excellent photoionization cross-section.

The objectives of the study were 1) to examine what effect pH would have on the adsorption of Cr^{3+}, 2) to determine if the clays would also behave as nucleation centers at or near the pH of precipitation of Cr^{3+} and 3) to examine the plot of the Si/Cr ratio versus the pH of adsorption and determine if it is similar to that of Si/Co.

Adsorption experiments were performed at pH values

of 2, 4, 6, 8, and 10. The solution concentration data for these experiments appears in Tables XIII and XIV. The major dissolved species for 100 ppm solutions at pH 2 are $Cr(H_2O)_6^{3+}$(93.5%) and at pH 4 $Cr_2(OH)_2^{4+}$(91%). At pH values 6, 8, and 10 the precipitation of chromium hydroxide was anticipated. Visible evidence of a blue green precipitate was noted at each of these pH values. The dissolved chromium content calculated from a K_{sp} value of 3.2×10^{30} for a 100 ppm solution at pH 6 is 3.16×10^{-7}M, at pH 8 3.16×10^{-9}M, and at pH 10 3.16×10^{-11}M. The measured chromium content of the sample aliquots for the experiments at pH 6, 8, and 10 indicated that no chromium was present.

At pH 2, 3.5 milliequivalents of chromium per 100 grams of clay was adsorbed on ripidolite and kaolinite. At pH 4, 7.0 milliequivalents of chromium per 100 grams of clay was adsorbed on ripidolite while 14.0 milliequivalents of chromium per 100 grams clay was adsorbed on kaolinite. At pH 6, 8, and 10 virtually all of the chromium had precipitated as the insoluble chromium hydroxide.

As with cobalt, the amount of chromium adsorbed increased with increasing pH. However, cobalt showed no appreciable adsorption as indicated for the AA data in the range where the chromium was adsorbed, indicating that the charge of the cation may play an important role in the pH at which it is adsorbed.

The Cr $2p_{3/2}$ binding energies for Cr_2O_3, $Cr(OH)_3$,

Table XIII

Chromium Adsorption on Kaolinite at pH 2, 4, 6, 8, 10

	pH 2		pH 4		pH 6		pH 8		pH 10	
Max. pH	2.05		4.03		6.20		8.19		10.06	
Min. pH	1.93		3.77		5.55		7.65		9.89	
Avg. pH	1.99±.03		3.92±.05		5.90±.12		7.92±.18		9.99±.04	
Species Analyzed	I	F	I	F	I	F	I	F	I	F
SiO_2	0	1	0	0	0	1	0	0	0	0
Cr	101	98	101	89	0	0	0	0	0	0
Fe	1	0	0	0	0	0	0	0	0	0
Mg	2				1	3	0	1	0	1
K	0	0	0	1	0	1	0	0	0	1
Al	1	1	0	0	0	0	0	0	0	1

I is equal to Initial
F is equal to Final

Table XIV

Chromium Adsorption on Ripidolite at pH 2, 4, 6, 8, 10

	pH 2		pH 4		pH 6		pH 8		pH 10	
Max. pH	2.08		4.06		6.27		8.45		10.20	
Min. pH	1.97		3.79		5.64		8.01		9.80	
Avg. pH	2.02±.02		3.94±.08		6.00±.16		8.28±.14		10.02±.11	
Species Analyzed	I	F	I	F	I	F	I	F	I	F
SiO_2	0	9	0	5	0	1	0	0	0	1
Cr	100	97	98	92	0	0	0	0	0	0
Fe	1	9	0	2	0	0	0	0	0	0
Mg	2	46	3	25	1	22	0	12	0	1
K	0	1	0	1	0	1	0	1	0	1
Al	1	8	0	3	0	1	0	0	0	1

I is equal to Initial
F is equal to Final

$Cr(NO_3)_3\ 6H_2O$, volkanskoite, and chromium adsorbed at pH's 2, 4, 6, 8, and 10 on ripidolite and kaolinite are in Table XV.

Unlike the binding energies of cobalt, the binding energies of the chromium compounds compared favorably with those in literature [93, 102, 103]. Where possible, comparison of FWHM of the Cr $2p_{3/2}$ levels were made with those in literature also and were found comparable.

The Cr $2p_{3/2}$ binding energy of Cr^{3+} adsorbed on kaolinite and ripidolite at pH 6, 8, and 10 is 577.0±0.1 eV. As mentioned previously, $Cr(OH)_3$ or some chromium hydroxy compound had visibly precipitated at pH 6 and higher. The binding energy of Cr $2p_{3/2}$ in $Cr(OH)_3$ is 576.7±0.1 eV. Therefore, although the binding energies do not compare exactly, they are nearly within experimental precision of each other. This evidence, coupled with the observation of a visible precipitate, indicates that $Cr(OH)_3$ or some chromium hydroxy compound has been adsorbed or associated with the clay surface.

The Cr $2p_{3/2}$ binding energy of Cr^{3+} adsorbed on kaolinite and ripidolite at pH 2 is 577.4 eV and 577.1 eV respectively. The chromium binding energies are approximately 1.0 eV lower than those determined for lattice chromium in volkanskoite, uvarorite,[93] and kämmerite,[93] so it can be concluded that the adsorbed chromium has not penetrated into a lattice site. Also comparison of the Cr $2p_{3/2}$ binding

energy of the adsorbed Cr^{3+} shows that it is neither $Cr(OH)_3$ or Cr_2O_3. Although, it can be concluded as to what species of Cr^{3+} is not adsorbed on the surface, it cannot be conclusively proven what species of Cr^{3+} is adsorbed on the surface from XPS data alone. Possibly, examination of the Cr^{3+} adsorbed on the surface using UV-visible spectroscopy could aid in the determination of the species on the surface.

The XPS data can be helpful, however, in describing how the cation might be bonded to the surface. In the previous section on Co^{2+} adsorption, it was mentioned that the clay surface is considered to be negatively charged. Koppelman suggested that the cation when adsorbed would have a negative charge donated to it from the clay surface, thereby lowering the binding energy of the adsorbed cation. If this is true, then the ripidolite clay surface is more highly charged that the kaolinite clay surface as demonstrated by the lowering of the Cr $2p_{3/2}$ binding energy by about 0.3 eV.

At pH 4, the Cr $2p_{3/2}$ binding energy for Cr^{3+} adsorbed on kaolinite and ripidolite are 577.4 eV and 577.3 eV, respectively. The Cr $2p_{3/2}$ binding energy is about 1.0 eV lower for adsorbed Cr^{3+} than that determined for lattice Cr^{3+}. Therefore, it can also be concluded that lattice penetration has not occurred at pH 4. Comparison of the Cr $2p_{3/2}$ binding energy of the adsorbed Cr^{3+} shows that it is neither $Cr(OH)_3$ or Cr_2O_3.

Table XV

Chromium Binding Energies
(Cr $2p_{3/2}$ level)±0.1 eV

	Binding Energy	FWHM
Cr_2O_3	576.5	3.1
$Cr(OH)_3$	576.7	3.0
$Cr(NO_3)_3 \cdot 9H_2O$	577.8	3.2
Volkanskoite	578.1	3.2
Uvarorite	578.3[93]	3.1
Kämmerite	578.2[93]	3.2

	Chromium Adsorbed on Kaolinite	FWHM	Chromium Adsorbed on Ripidolite	FWHM
pH 2	577.4	3.8	577.1	3.8
pH 4	577.4	3.4	577.3	3.2
pH 6	577.0	3.1	577.1	3.1
pH 8	577.1	2.9	577.0	3.2
pH 10	577.0	3.0	577.0	3.2

Conclusive identification of the species of Cr^{3+} on the surface is not possible. At pH 4, solution data indicates the major species of Cr^{3+} in solution is a dimer, $Cr_2(OH)_2^{4+}$. Yet, little or no change in the binding energy of the adsorbed species occurs from pH 2, to pH 4. This only further points out the need for further study by other methods such as reflectance UV-visible in order to determine the species of Cr^{3+} on the surface.

The $^{Cr}/Si$ ratio was determined by XPS. The $^{Cr}/Si$ ratio was determined from the equation:

$$^{Cr}/Si = {}^{RI}\,Cr/RI_{Si}$$

where RI_{Cr} represents the relative intensity of the chromium phtotpeak calculated from a photoionization cross-section of 7.60.[99]

The $^{Cr}/Si$ ratios are in Table XVI and a comparison with the $^{Co}/Si$ (Fig. 12 and 13) and $^{Cr}/Si$ (Fig. 16 and 17) graphs show the same trends, ie. that they increase in adsorption as they near the pH of precipitation. This indicates that in solution, both cations exhibit similar behaviour when they near the pH of precipitation of the hydroxy species. This is further confirmed when a comparison of the Cr^{3+} removed from solution as determined by atomic absorption is plotted against pH (Fig. 15).

Also at pH 6, 8, and 10 the Cr^{3+} has completely precipitated onto the surface of the clays. However, the

Table XVI

Cr/Si Ratio for Chromium Adsorbed on Kaolinite and Ripidolite

pH	Cr/Si Ratio for Cr^{3+} Adsorbed on Kaolinite ($x10^{-3}$)	Cr/Si Ratio for Cr^{3+} Adsorbed on Ripidolite ($x10^{-3}$)
2	9.3	8.3
4	10.3	22.2
6	18	285
8	26	500
10	24	500

Cr-ratio at pH 6 is about one half the Cr-Si ratios at pH 8 and 10. This might be explained by some sort of particle orientation for the $Cr(OH)_3$ on the clay surface which diminishes the intensity of the Cr $2p_{3/2}$ photopeak.

E. Adsorption of Ba^{2+} on Ripidolite and Kaolinite

The study of Co^{2+} raised many questions as to how a cation may be bound to the surface of a clay. For ripidolite, the Co $2p_{3/2}$ binding energy was seen to increase in increments of about 0.4 eV. But for kaolinite below pH 8, the binding energy remained the same. It was of interest then, to study a cation not common to the clay which did not precipitate or undergo hydrolysis over the pH range indicated to determine if changes in the clay surface occurred because of pH changes and if these changes would have any effect on the binding energy of the adsorbed cation.

Therefore, a study of the adsorption of Ba^{2+} onto the clay minerals was undertaken. Ba^{2+} was selected for study because calculation from the K_{sp} equilibrium constant showed that a 100 ppm Ba^{2+} solution would not precipitate as $Ba(OH)_2$ before pH 14. An added advantage to the study was the high photoionization cross-section of the $3d_{3/2,5/2}$ levels of Ba^{2+}. This large cross-section meant that the Ba XPS signal would be large for Ba^{2+} on the surface as compared to Co^{2+} and Cr^{3+}.

The Ba $3d_{5/2}$ binding energies for BaO, $Ba(OH)_2$,

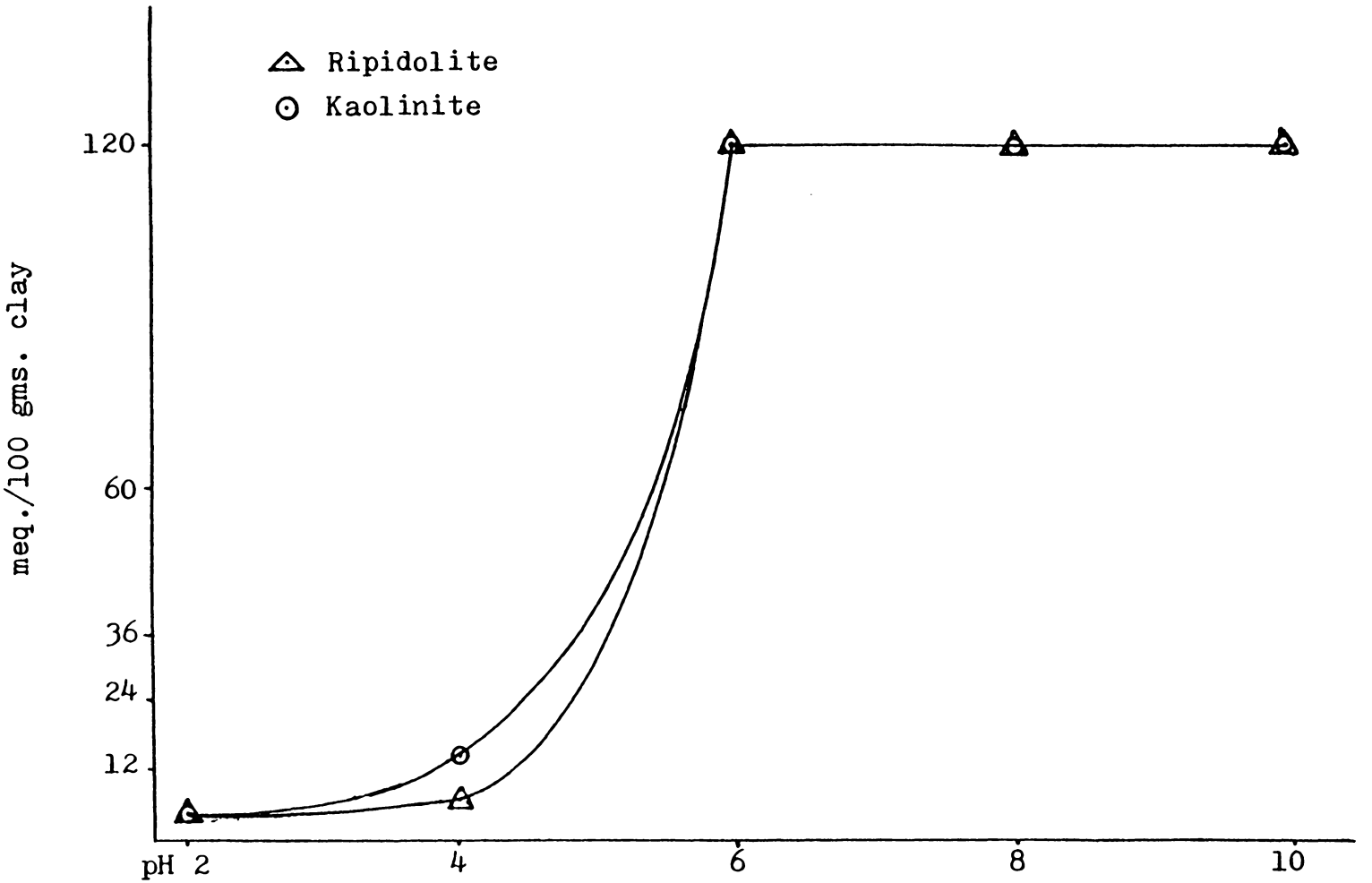

Figure 15. Uptake of Cr^{3+} by kaolinite and ripidolite

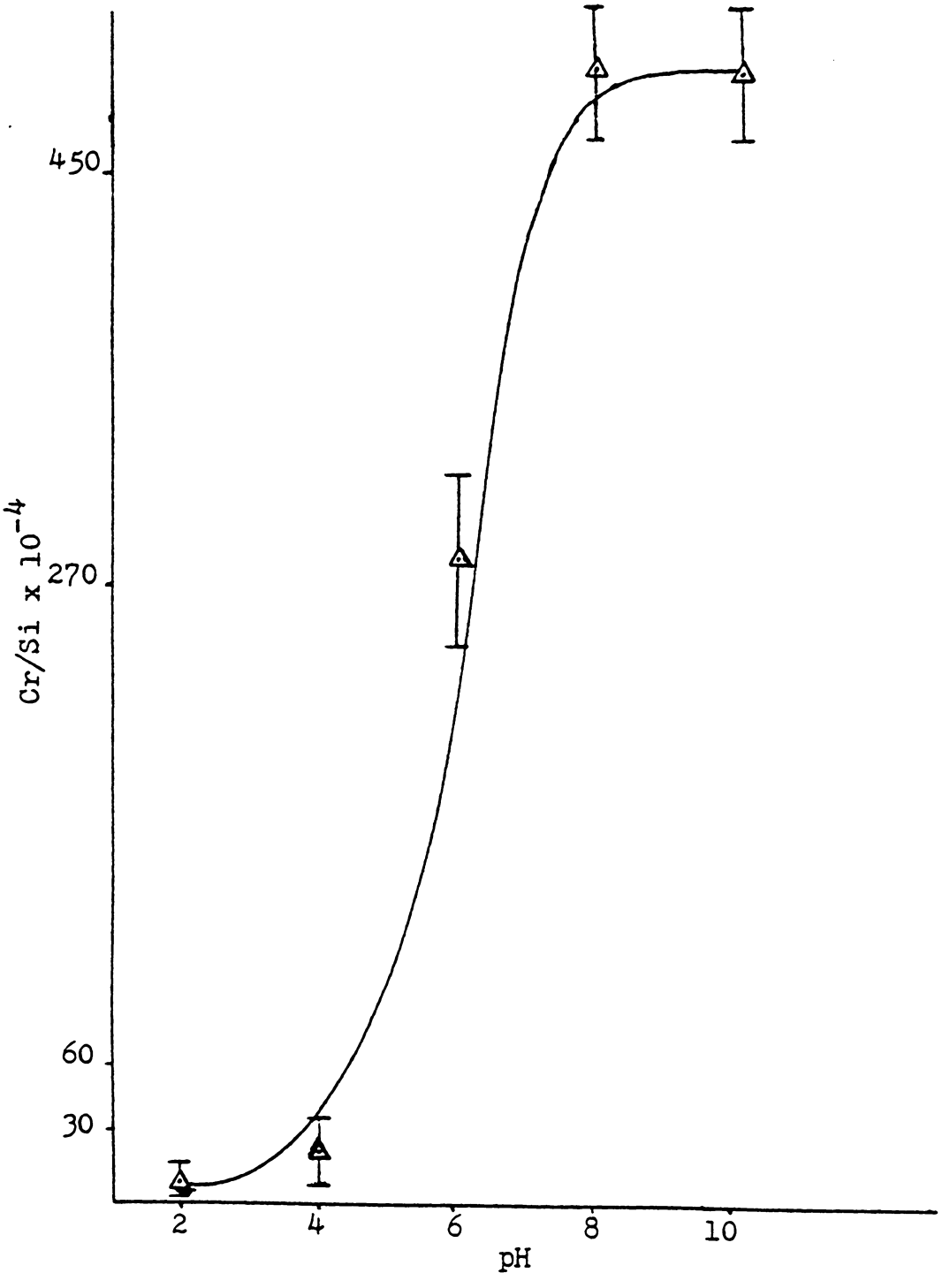

Figure 16. Uptake of Cr^{3+} by ripidolite

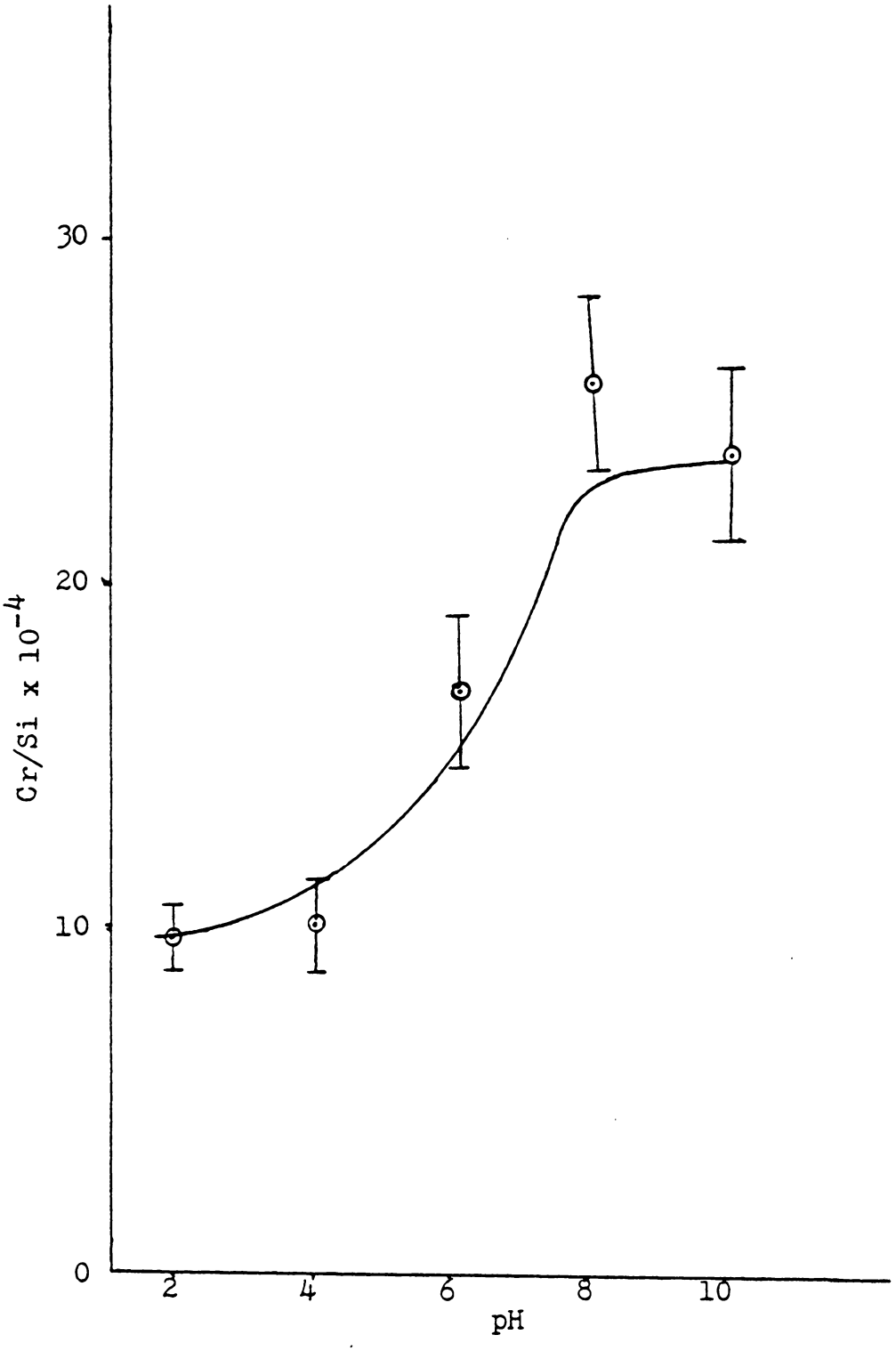

Figure 17. Uptake of Cr^{3+} on kaolinite

$Ba(NO_3)_2$ and for Ba^{2+} adsorbed at pH 2, 4, 6, 7, 8, and 10 on ripidolite and kaolinite are in Table XVII.

Little work on group IIA elements, has been done, most of which has focused on magnesium, beryllium, and calcium. No literature values of the pure barium compounds studied could be found for comparison.

The Ba $3d_{5/2}$ binding energy for Ba^{2+} adsorbed on kaolinite was 781.0±0.1 eV. The binding energy did not change throughout the pH range for the adsorption experiments. The Ba $3d_{5/2}$ binding energy of Ba^{2+} adsorbed on ripidolite was 780.5±0.1 eV. This binding energy also remained the same for all adsorption experiments performed on ripidolite. Because changing the pH did not affect the binding energy of the adsorbed Ba^{2+}, it can be concluded that the adsorption sites do not change in nature as pH changes or that if they do change, that these changes do not affect the binding energy of the adsorbed Ba^{2+}. It is probable then that the binding energy changes for Co^{2+} adsorbed on ripidolite at pH 4, 6, and 7 is due to either changes in species adsorbed on the surface or that the Co^{2+} cation undergoes some specific interaction with the clay that is unique to itself.

Also of interest is the binding energy difference of 0.5 eV between Ba^{2+} adsorbed on kaolinite and Ba^{2+} adsorbed on ripidolite. This is greater than the 0.3 eV difference between Cr^{3+} adsorbed on kaolinite and ripidolite.

Table XVII

Barium Binding Energies
(Ba $3d_{5/2}$ level) ±0.1 eV

	Binding Energy	FWHM (eV)
BaO	780.2	2.9
$Ba(OH)_2$	780.5	3.0
$Ba(NO_3)_2$	780.8	2.1

pH Adsorption	Binding Energy of Ba^{2+} Adsorbed on Kaolinite	FWHM (eV)	Binding Energy of Ba^{2+} Adsorbed on Ripidolite	FWHM (eV)
2	781.0	2.3	780.5±.2 eV	3.0
4	781.0	2.4	780.6±.1 eV	2.4
6	781.0	2.4	780.5	2.4
7	781.0	2.4	780.5	2.4
8	781.0	2.5	780.5	2.4
10	780.8	2.4	780.5	2.4

One theory of the adsorption phenomomen involves a negative charge donation from the surface of the clay to the cation, so it might be expected that a trivalent cation with its greater charge might have a greater binding energy difference than a divalent one. A possible explanation for barium's apparent anomalous behavior might be related to its size and hydration energy. The chromium and cobalt ions have a high charge over a small area, therefore, the coordinated waters are more tightly bound than they would be for a large cation such as Ba^{2+}. If the waters of hydration do interfere with the adsorption process, a simple experiment to validate this might be performed. The ions, Mg^{2+}, Ca^{2+}, Sr^{2+}, and Ba^{2+} would all be allowed to react with the clays. The binding energy difference between the cations adsorbed on each clay would be expected to follow the trend of the hydration energies of the cations. That is, the higher the hydration energy of a cation, the lower the binding energy difference between the cation adsorbed on each clay.

The bonding difference between Ba^{2+} adsorbed on kaolinite and ripidolite can also be related to the charge density on the surface of the clays. The charge density of the surface of the clay can be calculated from the equation:

$$\text{charge density on the clay surface} = \frac{(CEC)(A)(B)}{SA}$$

where CEC represents the cation exchange capacity in miliequivalents per 100 grams, A represents Avogadro's

number, B represents the charge on an electron in e.s.u., and SA represents the surface area of the clay in m^2/gm. The charge density for ripidolite is about 3.4 times that of kaolinite as calculated from the data in Table III. Therefore the lower binding energy of ripidolite is due to the greater charge density which allows it to donate more negative charge to the adsorbed cation.

Although no data on how much Ba^{2+} had been removed from solution was gathered, the $^{Ba}/_{Si}$ ratio was calculated to compare with $^{Co}/_{Si}$ and $^{Cr}/_{Si}$ ratios. The $^{Ba}/_{Si}$ ratio was calculated from the equation:

$$^{Ba}/_{Si} = {}^{RI_{Ba}}/_{RI_{Si}}$$

where RI_{Ba} is the relative intensity of the Ba $3d_{5/2}$ peak and RI_{Si} is the relative intensity of the Si $2p_{1/2}, 2p_{3/2}$ peak. The Ba $3d_{5/2}$ peak has a cross-section of 24.75.[99] The $^{Ba}/_{Si}$ ratio for Ba^{2+} adsorbed on kaolinite and ripidolite is in Table XVIII and is plotted against the pH of the adsorption experiment. (Fig. 16).

The plots of $^{Cr}/_{Si}$ and $^{Co}/_{Si}$ did not cover the entire pH range without precipitation of the hydroxy species occurring. But, as the plots of the other ratios had demonstrated, adsorption increases with increasing pH.

Table XVIII

$^{Ba}/_{Si}$ Ratio for Barium Adsorbed on Kaolinite and Ripidolite

pH	$^{Ba}/_{Si}$ Ratio for Ba^{2+} Adsorbed on Kaolinite ($x10^4$)	$^{Ba}/_{Si}$ Ratio for Ba^{2+} Adsorbed on Ripidolite ($x10^4$)
2	4.53	17.3
4	48.5	40.2
6	63.3	166
7	119	189
8	102	192
10	192	500

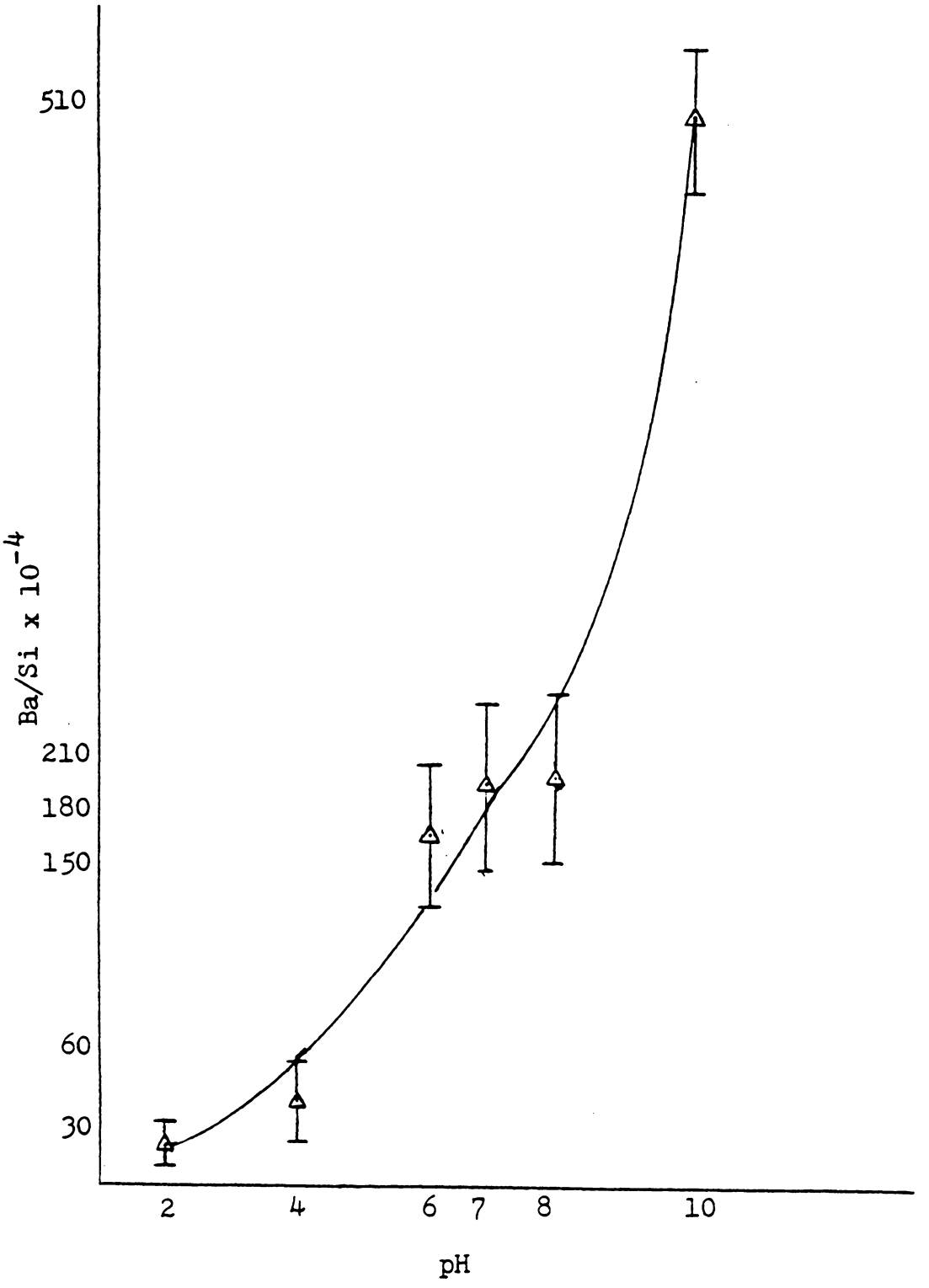

Figure 18. Uptake of Ba^{2+} by ripidolite

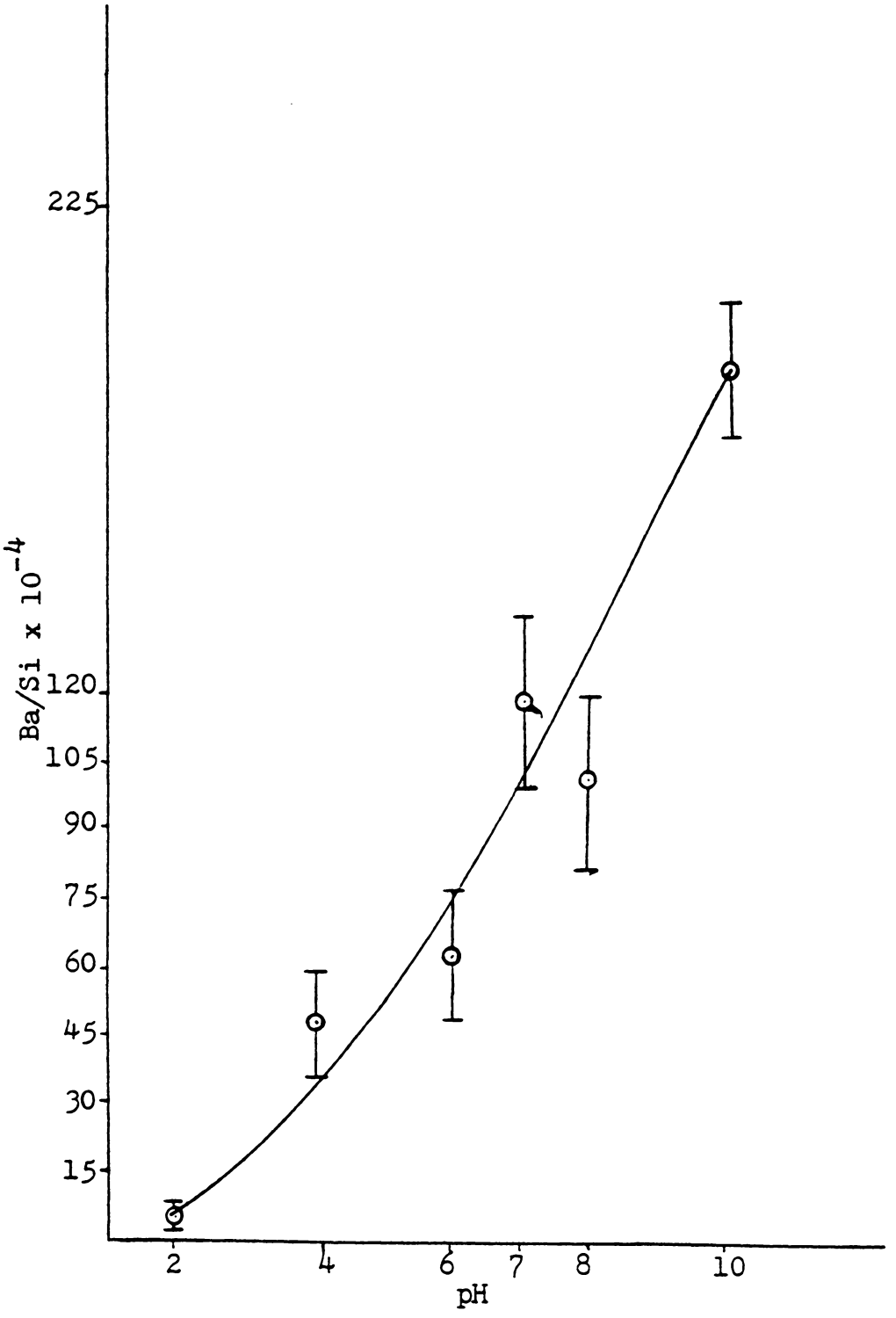

Figure 19. Uptake of Ba^{2+} by kaolinite

5. SUMMARY

Cation adsorption might be looked upon as analogous to using small probes to investigate a clay surface. Each cation has different properties which when investigated thoroughly help to identify properties of the surface and its effect on the adsorbed cation. By combining the information from each of three systems, a more complete picture of what has occurred in each might be obtained.

The following is a summary of the facts.

1.) The Co $2p_{3/2}$ binding energy Co $2p_{1/2}$-Co $2p_{3/2}$ splitting and FWHM for Co^{2+} on ripidolite at pH 7, 8, and 10 and on kaolinite at pH 8 and 10 are the same as for $Co(OH)_2$.

2.) The Co $2p_{3/2}$ binding energy for Co^{2+} on ripidolite at pH 4, 6, and 7 changes by 0.4 eV with each change in pH, but the Co $2p_{1/2}$-Co $2p_{3/2}$ splitting and FWHM remain the same at pH 6 and 7.

3.) The Co $2p_{1/2}$-Co $2p_{3/2}$ splitting was approximately 15.0 eV for Co^{2+} adsorbed on kaolinite at pH 4, 6, and 7 and on ripidolite at pH 2, and 4.

4.) The Co $2p_{1/2}$ satellite is of greater intensity than the main photopeak for Co^{2+} adsorbed on kaolinite at pH 2, 4, 6, and 7 and on ripidolite at pH 2 and 4. As the pH decreases, the satellite increases in intensity for Co^{2+} adsorbed on kaolinite.

5.) The Cr $2p_{3/2}$ binding energy, and FWHM for Cr^{3+} on ripidolite at pH 6, 8, and 10 and on kaolinite at pH 6, 8, and 10 is the same as that for $Cr(OH)_3$.

6.) The Ba $3d_{5/2}$ binding energy did not change as a function of pH for Ba^{2+} adsorbed on kaolinite or ripidolite.

7.) The binding energy of the Ba $3d_{5/2}$ level peak for Ba^{2+} adsorbed on ripidolite was 0.5 eV less than that for kaolinite.

Koppelman[93] proposed that a cation adsorbed on the negatively charged clay surface would have some of that negative charge transfered to the cation, thereby reducing the binding energy of the cation. Using this simple model, several conclusions about the clay surfaces can be reached. First, it appears that the ripidolite surface has a greater negative charge than kaolinite. This fact is also apparent from the calculation of the charge density for ripidolite and kaolinite. Second, neither clay surface has any effect on the Ba $3d_{5/2}$ binding energy as the pH changes. This means that any change in binding energy by Co^{2+} or Cr^{3+} when adsorbed is probably due to a change in species. If this is true, then kaolinite does not cause the precipitation of Co^{2+} or Cr^{3+} much before the expected pH of precipitation. As for ripidolite, $Co(OH)_2$ precipitation begins by pH 7, almost a full pH unit below its expected value. Also at pH 4 and pH 6 it appears that two different species of Co^{2+} may be adsorbed on ripidolite. And between pH 2 and pH 4, the Co $2p_{1/2}$, Co $2p_{3/2}$ splitting changes from approximately 16.0 eV to 15.0 eV. This might be due to the continuing loss of pH dependent charge. However, if the charge does change significantly

because of pH, it would seem that it would affect the Ba 3d $_{5/2}$ binding energy on ripidolite. Because it does not, it is difficult to discern why these effects occur.

6. REFERENCES

1. Goldberg, E. D., The Changing Chemistry of the Oceans, D. Dryssen and D. Jagner, eds., Wiley Interscience, New York, 1972.

2. Kennedy, V. C., U. S. Geol. Sur. Prof. Paper 433-D, 1965.

3. Gibbs, R. J., Geol Soc. Amer. Bull., 78, 1203 (1967).

4. Khar Kar, D. P., K. K. Turekian, and K. K. Bertine, Geochim. Cosmochim. Acta, 32, 285 (1968).

5. Chester, R. and J. P. Riley, Introduction to Marine Chemistry, Academic Press, London, (1971).

6. Grim, R. E., Clay Mineralogy, McGraw-Hill, New York, 2nd ed. (1968).

7. Weaver, C. E. and L. D. Pollard, The Chemistry of Clay Minerals, Elsevier, Amsterdam. (1973).

8. Pauling, L., Proc. Nat'l. Acad. Sci., U. S. 16, 57B (1930).

9. Gruner, J. W., Z. Krist., 83, 75 (1932).

10. Brindley, G. W. and K. Robinson, Min. Mag., 27, 242 (1946).

11. Brindley, G. W. and D. M. C. MacEwan, X-ray Identification and Structure of Clay Minerals, Mineralogical Society of Great Britain. Monograph, 87, (1961).

12. Newnham R. E., Min. Mag. 32, 683 (1961).

13. Brindley, G. W. and M. Nakahira, Min. Mag, 31, 781 (1958).

14. Bailey, S. W., Am. Mineral., 1196 (1963).

15. Mauguin, C. H., Bull. Soc. Franc. Mineral., 53, 279 (1930).

16. McMurchy, R. C., Z. Krist., 88, 420 (1934).

17. Kelly, W. P., Cation Exchange in Soils, Reinhold, N. Y. (1948).

18. Thompson, H. S., J. Roy. Agr. Soc. Engl., 11, 313 (1850).

19. Way, J. T., J. Roy. Agr. Soc. Engl., 11, 313 (1850).

20. Way , J. T., J. Roy. Agr. Soc. Engl., 13, 123 (1852).

21. Wilklander, L. in Chemistry of the Soil, F. E. Bear (ed.), Reinhold. Publ. Corp., New York, (1964).

22. Schofield, R. K. and H. R. Somson, Clays Clay Miner., 2, 45 (1953).

23. Swartzen-Allen, S. L. and E. Matijevic, Chem. Rev., 74, 385 (1974).

24. Shainberg, I. and W. D. Kemper, Soil Sci., Soc. Amer. Proc. 30, 707 (1966).

25. Shainberg, I. and W. D. Kemper, Soil Sci., Soc. Amer. Proc., 30, 700 (1966).

26. Shainberg, I. and W. D. Kemper, Clays Clay Miner., 14, 117 (1965).

27. Banin, A., Isr. J. Chem., 6, 27 (1968).

28. Kaddah, M. T., Soil Sci., 106, 67 (1968).

29. Tamers, M. A. and H. C. Thomas, J. Phys. Chem. 64, 29 (1960).

30. Juo, A. S. R. and S. A. Barber, Soil Sci., 109, 143 (1970).

31. Hodgson, J. F., Soil Sci. Soc. Amer. Proc., 24, 165 (1960).

32. Gilbert, M., Soil Sci. 109, 23 (1970).

33. Wild, A. and J. Keag, J. Soil Sci. 15, 135 (1964).

34. Clark, J. S., Can. J. Soil Sci. 50, 85 (1970).

35. Uskova, E. T., E. G. Vasilev and I. A. Uskov, Colloid J. USSR, 30, 118 (1968).

36. Gal, M. and C. I. Rich, Clays Clay Miner., 20, 175 (1972).

37. Lin, C. and N. T. Coleman, Soil Sci. Soc. Amer. Proc. 24, 44 (1960).

38. Van Olphen, H. An Introduction to Clay Colloid Chemistry Interscience Publishers, New York, N. Y., (1963).

39. Carlson, R. M. and R. Overstreet, Soil Sci. 103, 213 (1967).

40. Farrah, H. and W. F. Pickering, Austral. J. Chem., 29, 1167 (1976).

41. Farrah, H. and W. F. Pickering, Austral. J. Chem., 29, 1177 (1976).

42. McBride, M. B., Soil Sci. Soc. Am. J., 40, 452 (1976).

43. McBride, M. B., Clays Clay Miner. 24, 88 (1976).

44. Jones, J. P. E., B. R. Angel, and P. L. Hall, Clays Clay Miner. 10, 257 (1974).

45. Murray, J. W., Geochim. Cosmochim. Acta, 39, 635 (1975).

46. Healy, T. H., R. O. James, and R. Cooper, Advan. Chem. Ser., 79, 62 (1968).

47. Tewari, P. H. and W. Lee, J. Colloid Interface Sci. 52, 77 (1975).

48. Hildebrand, E. E. and W. E. Blum, Naturwissenschaften, 61, 169 (1974).

49. Forbes, E. A., A. M. Posner, and J. P. Quirk, J. Colloid Interface Sci., 49, 403 (1974).

50. Swartzen-Allen, S. L. and E. Matijevic, J. Colloid Interface Sci., 50, 143 (1975).

51. Fordham, A. W., Austral, J. Soil Res., 11, 185 (1973).

52. Dugger, D. L., J. H. Stanton, B. M. Irby, B. L. McConnel, W. W. Cummings, and R. W. Maatman, J. Phys. Chem., 68, 757 (1964).

53. James R. O. and T. W. Healy, J. Colloid Interface Sci., 40, 42 (1972).

54. Siegbahn, K., C. Nordling, A. Fahlman, R. Nordberg, K. Hamrin, J. Hedman, G. Johansson, T. Bergmark, S.-E. Karlsson, I. Lindgren and B. Lindberg, Electron Spectroscopy for Chemical Analysis: Atomic, Molecular, and Solid-State Structure Studied by Means of Electron Spectroscopy, Almqvist and Wiksell, Stockholm, Sweden (1967).

55. Lindau, I. and W. E. Spicer, J. Electron Spectrosc. Related Phenom., 3, 409 (1974).

56. Klasson, M., A. Berndtsson, J. Hedman, R. Nilsson, R. Nyholm, and C. Nordling, J. Electron Spectrosc. Related Phenom., 3, 427 (1974).

57. Flitsch, R. and S. I. Raider, J. Vac. Sci. Tech., 12, 305 (1975).

58. Battye, F. L., J. Liesegang, R. Lecky, and J. G. Jenkin, Phys. Lett. A., 49, 155 (1974).

59. Swingle, II, R. S., and W. M. Riggs, CRC Crit. Rev. Anal. Chem., 5, 267 (1975).

60. Johanson, G. J. Hedman, A. Berndtsson, M. Klasson, and R. Nilsson, J. Electron Spectros. Related Phenom., 2, 295 (1973).

61. Huchital, D. A. and R. T. McKeon, Appl. Phys. Lett., 20, 158 (1972).

62. Dianis, W. P. and J. E. Lester, Anal. Chem., 45, 1416 (1973).

63. Ginnard, C. R. and W. M. Riggs, Anal. Chem 46, 1306 (1974).

64. Betteridge, D., J. C. Carver, and D. M. Hercules, J. Electron Spectrosc. Related Phenom. 2, 237 (1973).

65. Olgivie, J. L. and A. Wolberg, Appl. Spectrosc. 26, 401 (1972).

66. Vernon, G. A., G. Stucky and T. A. Carlson, Inorg. Chem., 15, 278 (1976).

67. Frost, D. C., C. A. McDowell and I. S. Woolsey, Mol. Phys. 27, 1473 (1974).

68. Yin., L. I., S. Ghose, and I. Adler, Science, 173, 633 (1971).

69. Adams, I., J. M. Thomas, and G. M. Bancroft, Earth Planet Sci. Lett., 16, 429 (1972).

70. Freund, F. and M. Hamich, Fortschur. Mineral., 48, 243 (1971).

71. Huntress, W. T. and L. Wilson, Earth Planet Sci. Lett., 15, 59 (1972).

72. Schultz, H. D., C. J. Vesely, and D. W. Langer, Appl. Spectrosc, 28, 374 (1974).

73. Counts, M. E., J. S. C. Jen, and J. P. Wightman, J. Phys. Chem., 77, 1924 (1973).

74. Koppelman, M. H. and J. G. Dillard, ASC Symp. Ser., 18, 186 (1975).

75. Koppelman, M. H. and J. G. Dillard, Clays Clay Miner. 25, 457 (1977).

76. Stucki, J. W. and C. B. Roth, Soil Sci. Am. J., 41, 808 (1977).

77. Stucki, J. W., C. B. Roth, and W. E. Baitinger, Clays Clay Miner., 24, 289 (1976).

78. Briggs, D. and Y. M. Bosworth, J. Colloid Interface Sci., 59, 194 (1977).

79. McIntyre, N. S. and P. H. Tewari, J. Colloid Interface Sci., 59, 195 (1977).

80. Lunsford, J. H., P. J. Hutta, M. J. Lin, and K. A. Windhorst, Inorg. Chem., 17, 606 (1978).

81. Sommer, S., Amer. Mineral., 60, 483 (1975).

82. McIntyre, N. S. and M. G. Cook, Anal. Chem., 47, 2208 (1975).

83. M. Oku, and K. Hirokawa, J. Electron Spectrosc. Related Phenom., 10, 103 (1977).

84. Nordberg, R., H. Brecht, R. G. Albridge, A. Falham, and J. R. Van Wazer, Inorg. Chem., 9, 2469 (1970).

85. Allen, G. C., M. T. Curtiss, A. J. Hooper and P. M. Tucker, J. C. S. Dalton Trans., 1675 (1973).

86. Wagner, C. D., Anal. Chem., 49, 1282 (1977).

87. Petrovic, R., R. A. Berner, and M. B. Goldhaber, Geochim. Cosmochim. Acta, 40, 537 (1976).

88. Adams, J. M., S. Evans, P. I. Reid, J. M. Thomas, and M. J. Walters, Anal. Chem., 49, 2001 (1977).

89. Bancroft, G. M., F. R. Brown, and W. S. Fyfe, Anal. Chem., 49, 1044 (1977).

90. Hercules, D. M., Anal. Chem., 48, 295R (1976).

91. Hercules, D. M., and J. C. Carver, Anal. Chem., 46, 133R (1974).

92. Koppelman, M. H. and J. G. Dillard, The Application of X-ray Photoelectron Spectroscopy to the Study of Mineral Surface Chemistry, Proceedings of the 6th International Clay Conf., Oxford, England (1978).

93. Koppelman, M. H., An X-ray Photoelectron Spectroscopic Study of the Adsorption of Metal Ions on Marine Clay Minerals, Ph. D. Thesis, V.P.I. & S.U., 1976.

94. Rich, C. I., Clays Clay Miner., 13, (1965).

95. Joint Committee on Powder Diffraction Standards, Selected Powder Diffraction Data for Minerals JCPDS, Philadelphia, 1st ed., 1974.

96. Post, J. L. and C. C. Plummer, Clays Clay Miner., 20, 271 (1972).

97. Anderson, P. R. and W. E. Swartz, Jr., Inorg. Chem., 13, 2293 (1974).

98. Coleman, N. T. and G. W. Thompson, Soil Sci. Soc. Am. Proc., 28, 187 (1964).

99. Scofield, J. H., J. Electron Spectrosc. Related Phenom., 8, 129 (1976).

100. Burness, J. H., An X-ray Photoelectron Spectroscopic Study of Cobalt (II) and Manganese (II) Schiff Base Compleses and Their Oxygenation Products, Ph. D. Thesis, V.P.I. & S.U., 1975.

101. Oku, M. K. Hirokawa and S. Ikeda, J. Electron Spectrosc. Related Phenom., 7, 465 (1975).

102. McGuire, G. E., G. K. Schweitzer and T. A. Carlson Inorg. Chem., 12, 2450 (1973).

103. Carver, J. C., G. K. Schweitzer, and T. A. Carlson, J. Chem. Phys., 57, 973 (1972).

The vita has been removed from the scanned document

ADSORPTION OF COBALT, CHROMIUM, AND BARIUM ON RIPIDOLITE AND KAOLINITE AS EXAMINED BY X-RAY PHOTOELECTRON SPECTROSCOPY

by

Adrian Bruce Emerson

(ABSTRACT)

X-ray photoelectron spectroscopy (XPS) has been used to study the bonding of adsorbed metal cations to clay minerals. Binding energy differences of the adsorbed metal cations can be related to changes in the electron density or charge on the atom of interest.

Adsorption experiments were carried out in aqueous solution at controlled pH's of 2, 4, 6, 8, and 10 for Ba^{2+}, Co^{2+}, Cr^{3+}, adsroption on the clays kaolinite and ripidolite.

Solution processes were monitored by measuring the solution concentrations of dissolved silica and the metal ions Fe^{3+}, Mg^{2+}, K^{+}, Al^{3+}, Cr^{3+}, and Co^{2+} at the beginning and the end of the experiment. Atomic absorption spectroscopy was used to determine the metal ion concentrations and dissolved silica was determined spectrophotometrically as a molybdate complex.

Examination of the adsorbed cation species on the clay surface by XPS indicated that the clays behaved as nucleation centers at or near the pH of precipitation of the cations. Further it was found that high spin Co^{2+} in solution became

low spin Co^{2+} or formed a highly covalent bond when adsorbed on kaolinite at pH's 4, 6, and 7 and on ripidolite at pH 2 and 4. Finally, if the clay has a negatively charged surface which donates some of its charge to the positive cation, then the barium XPS data indicated that ripidolite has a greater negative surface charge than kaolinite. This idea was supported by calculations of the surface charge density from CEC and surface area data.